UCLouvain

epl

École polytechnique de Louvain

Contribution of visual and proprioceptive feedback to the control of arm movements :

Influence of the instruction on the integration of sensitive information.

Writer:**Sophie Ledoux**
Supervisors:**Frédéric Crevecoeur**
Readers:**Anne Hoffmann, Philippe Lefèvre, Valéry Legrain, Renaud Ronsse**
Academic year 2021–2022
Master [120] in Biomedical Engineering

Abstract

Multisensory integration in motor control has been widely studied for decades. Visual and proprioceptive feedback principally contribute to the estimation of the position of the arm and the dynamics of the environment. However, it remains unknown how vision and proprioception are integrated during online control when they convey incongruent information. Here, we analyzed the way that feedback from these modalities is integrated when participants were aware of the deviation between visual feedback and their true hand location during reaching movements under mechanical perturbations. To do this, participants realized two experiments with a similar protocol but different instructions. In one experiment, they were asked to control the hand-aligned cursor without knowing that it could be deviated from the actual position of their hidden hand. The second experiment consisted in asking them to control their hand, they were aware of the possibility of a deviation of the visual cursor. We observed that participants were not able to ignore the visual feedback even if they were aware of its incongruency and that they tended to have greater corrective responses when they had to control their hand rather than the visual cursor. We hypothesized that this increase in corrective response while controlling their hand is due to the inability of the participants to model the environment they were in, leading them to adopt a robust control strategy.

Acknowledgements

First, I would like to thank Professor F. Crevecoeur for his follow-up and his precious advices throughout this year. It was a real opportunity to be part of this lab and to share their passions.

I am particularly grateful to Anne Hoffmann who devoted a lot of her time to the successful completion of this work. Through regular follow-up and many wise advices, she was able to guide me throughout my research. She was a great presence on whom I could rely, answering all my questions and giving me feedback even at the very first stage of the work.

I would also like to thank Professor P. Lefèvre, Professor V.Legrain and Professor R. Ronsse for agreeing to be part of my thesis jury.

Obviously this research would not have been possible without the dedication of my 16 participants whom I thank extremely.

Last but not least, I would like to thank all my family and friends who helped me throughout my student life and especially during the writing of this thesis. I would like to say a special thank you to Victoire Stavaux who stayed by my side throughout this period of hard work and who motivated me from the very beginning to stay the course and concentrate on what I had to do. I would also like to thank Noémie Lapraille and Anais Van Meerbeck who have always been there in good and bad times.

Finally, to all the people who directly or indirectly played a role in bringing me to this final stage: thank you !

Contents

List of abbreviations

BR Brachioradialis
CCW Counter-Clockwise
CNS Central Nervous System
CW Clockwise
EMG electromyography
FF Force Field
LMM Linear Mixed Model
LQG Linear Quadratic Gaussian
MLE Maximum-likelihood estimate
OFC Optimal Feedback Control
PD Posterior Deltoid
PEC Pectoralis Major
TL Triceps Lateralis
VG Visual Gain

List of Figures

Chapter 1

Introduction and objectives

In everyday life, it is often necessary for us to make reaching movements. Whether it is a precise movement like picking up a pin or a larger one like moving a chair, we need to know our environment and be able to estimate where we are in it.
In order to do this, it is necessary to correctly integrate the multitude of sensory signals at our disposal, called multisensory integration and carried out by the Central Nervous System (CNS).

Multisensory integration is fundamental for accurate movement control and therefore it is very important to understand how it works. Many studies are being carried out on this subject, raising different challenges related to changing sensory input, fast time scale of feedback responses despite sensory delay times, etc. Understanding exactly how the central nervous system integrates the various sensory information that surrounds us and how it handles disturbances would make it possible to develop the detection of certain neurological disorders. It would also allow us to improve the multisensory rehabilitation products used after a stroke or other neurological movement disorders. [1] Finally, it also opens the doors to affordable rehabilitation systems particularly requested for the elderly. [2]

1.1 Outline

This thesis will start with the state of the art on motor control, multisensory integration and causal inference in chapter 2. These are the building blocks of the theory needed to understand this work. After this, chapter 3 will include all the information about the experiments carried out. Results extracted from these experiments will be summarized in the chapter 4. Finally, all these results will be discussed in the chapter 5 of this thesis as well as a brief conclusion on the important points to be retained from this study.

Chapter 2

State of the art

2.1 Motor control

Throughout time, human beings are required to make movements. Whether they are voluntary or involuntary, precise or confused, all these movements reflect complex interactions between the CNS and the limbs. [3] Motor control studies the ability of the CNS to generate a command to the muscles to achieve this kind of goal-directed movement. Biological control is a hierarchical organization on three levels (3B's) : The **B**ehavior (movement characteristics linked to the task), the **B**iomechanics (mechanical properties of the musculoskeletal system) and the **B**rain (neural activity).(Figure 2.1.1)

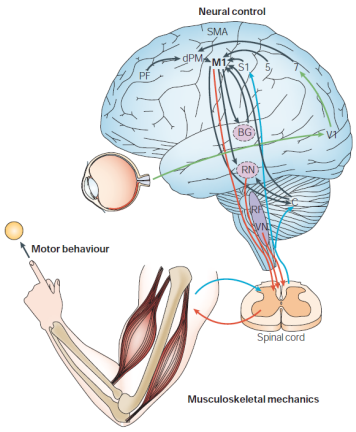

Figure 2.1.1 – Three levels of the biological control. The biological motor control is a hierarchical organization on three levels that interact. First, the behavior level corresponding to the observed action linked to the task. Then, the biomechanics of the limb to perform this task. Finally, the brain where neural control is performed. [3]

This interaction between the three levels can be described by the optimal feedback control theory.

Optimal feedback control

The Optimal Feedback Control is a mathematical model which aims to study the control signals that will optimize a certain performance while satisfying dynamic constraints of a dynamic system. [4][5]

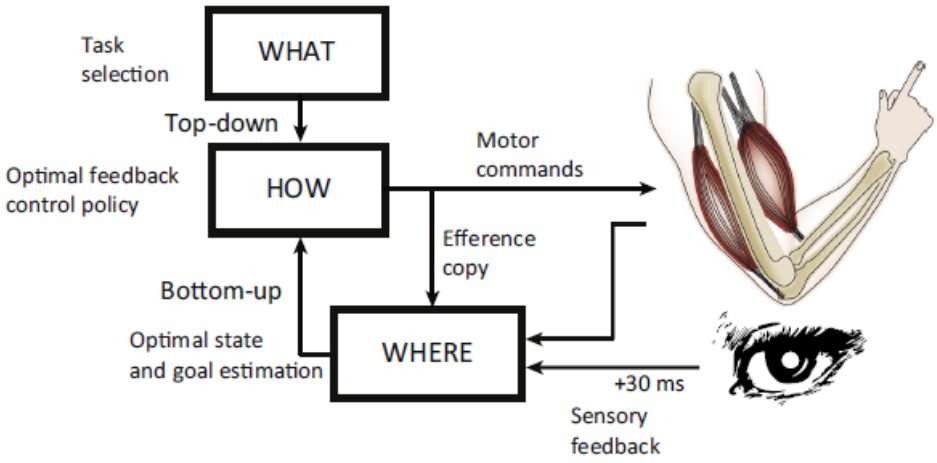

Figure 2.1.2 – Optimal Feedback Control WHAT : It is the goal of the behavior, overall objective of the motor system defined voluntarily. WHERE : Sensory feedback and efference copy signals of motor commands are combined to specify the present state of the world. HOW : The control policy defines what motor command should be generated based on the present state of the body and goal.[5]

This mathematical approach is a combination of two sources of information : an instantaneous multimodal estimation of the current state of the world based on feed-forward motor prediction and feedback sensory integration.(See figure 2.1.2) [6, 7]

Indeed, a voluntary movement is firstly governed by a task to be performed. This action will be done by minimizing a cost function considering the error and motor command (top-down processing).
Secondly, an optimal state estimation formed based on sensory feedback and the efference copy enter the motor controller to deliver the correct motor command to the limb (bottom-up). This efference copy refers to predicting the sensory impact of a given motor command by simulating the dynamics of the system over one time step. Both sources of information enter the CNS acting as a controller which uses an internal representation of the movement dynamics of the system to compute the command system [8]. A frequently used model of optimal control is the Linear Quadratic Gaussian (LQG) control.[9]

LQG feedback control is a neural feedback control that minimizes the cost of the movements while considering a noisy system.[10] $\mathbf{L}$ stands for the linear dynamics in state and control variables, $\mathbf{Q}$ stands for the quadratic cost function to be minimized and $\mathbf{G}$ stands for the zero-mean Gaussian noise variables ($\mathcal{N}(0, \sigma^2)$). In the framework of LQG control,

the control system can be defined as :

$$x_{k+1} = Ax_k + Bu_k + \epsilon_k$$

$$y_k = Hx_k + \omega_k$$

With the state vector at a certain time (x_{k+1}) a linear combination of the state at the previous time (x_k), the control vector (u_k) and a stochastic disturbance (ϵ_k). The observed state vector (y_k) is a linear combination of the true state vector and a stochastic disturbance (ω_k).
The cost function to be minimized can be written as :

$$J_k\left(x_k, u_k\right) = x_k^T Q_k x_k + u_k^T R u_k, \quad Q_k \geq 0, \quad k = 1, 2, \ldots, N-1,$$

$$J_N\left(x_N\right) = x_N^T Q_N x_N. \qquad R > 0.$$

The optimal control problem is to find a control sequence u_k that minimize this cost function J . For the fully observable case assuming a perfect knowledge of the state vector, the solution of the optimal control problem is a linear state feedback controller and a cost-to-go at each time step t given by : $v_k(x_k, u_k) = x_k^T S_k x_k + s_k$.
In biology control, we do not have perfect knowledge of the state vector, we are talking about state estimation ($\hat{x}_k$). It is assumed that this state estimation is a combination of priors and feedback.

Priors is everything we know about the state : $\hat{x}_{k+1}^{prior} = A\hat{x}_k + Bu_k$. It is in fact the estimation of the state vector through the dynamics of our system which we consider without noise thanks to the hypothesis of the Gaussian distribution centered in 0.
The feedback is the difference between observed state (what I get) and estimate at the previous step (what I expected) : $y_k - H\hat{x}_k$.
We thus have the estimated state : $\hat{x}_{k+1} = A\hat{x}_k + Bu_k + K\left(y_k - H\hat{x}_k\right)$.

The internal estimate of the state of a variable (such as hand location) is fundamental in motor control. Therefore it is important to minimize the variance of this estimation by minimizing the variance of the uncertainty of the system dynamics. [11] One way our CNS has found to reduce the error in the estimation of the surrounding environment is to combine information from multiple sensory modalities. [12]

2.2 Optimal cue combination

As explained, our ability to make decisions about our environment depends on the available sensory data and a prior knowledge about the current state of the world. These

afferent sensory inputs often come from multiple sources or modalities and are called sensory cues.
The way multisensory cues are integrated during motor control has already been studied a lot. [7, 11, 13, 14] A key aspect that is pervasive in these studies is the uncertainty of noisy sensory input. This uncertainty comes from the transformation of the physical stimulus into messages carried by noisy apparatus (neurons) and by the uncertainty of the stimulus itself. The cue uncertainty is measured by its variance. [15] Now how are these sensory cues optimally combined in order to minimize the estimation variance ? There are two different approaches leading to the same conclusions : the frequentist approach and the bayesian one.

Frequentist approach : Maximum Likelihood Estimation (MLE)

A first approach of optimal cue integration was based on the Maximum Likelihood estimation. [10] The basic principle is that each sensory modality is given a relative weight that is (inversely) proportional to its (variance) reliability.
Imagine $X \sim \mathcal{N}(\mu, \sigma_X^2)$ and $Y \sim \mathcal{N}(\mu, \sigma_Y^2)$ two sensory signals from different sources. From MLE theory, the combined mean and variance of these sensory cues is defined as:

$$\hat{\mu} = \alpha X + (1 - \alpha)Y$$

$$\sigma_{XY}^2 = \alpha^2 \sigma_X^2 + (1 - \alpha)^2 \sigma_Y^2$$

The aim is to minimize the total variability thus we obtain :

$$\alpha = \frac{\sigma_Y^2}{\sigma_X^2 + \sigma_Y^2}, \quad \sigma_{XY}^2 = \frac{\sigma_X^2 \sigma_Y^2}{\sigma_X^2 + \sigma_Y^2}$$

By taking the inverse of the variance as indicative of the signal reliability, we also obtain:

$$\alpha = \frac{1/\sigma_X^2}{1/\sigma_Y^2 + 1/\sigma_X^2}$$

Ernst & Banks [13] studied the interaction between visual and haptic feedback during tasks where the visual noise of the signals (and therefore the visual cue reliability) varied. The principle they demonstrated is that the reliability of a sensory cue and thus by extension its variability will define the dominance of this modality in the control process. Given the Maximum-likelihood estimate (MLE) theory they defined :
$S = \sum_i w_i S_i$ with $w_i = \frac{\frac{1}{\sigma_i^2}}{\sum_j \frac{1}{\sigma_j^2}}$ and the total variance of the estimate as : $\sigma_{VH} = \frac{\sigma_V^2 \sigma_H^2}{\sigma_V^2 + \sigma_H^2}$
Where S is the physical property that is estimated and σ_V, σ_H are respectively the vision

and haptic variances.

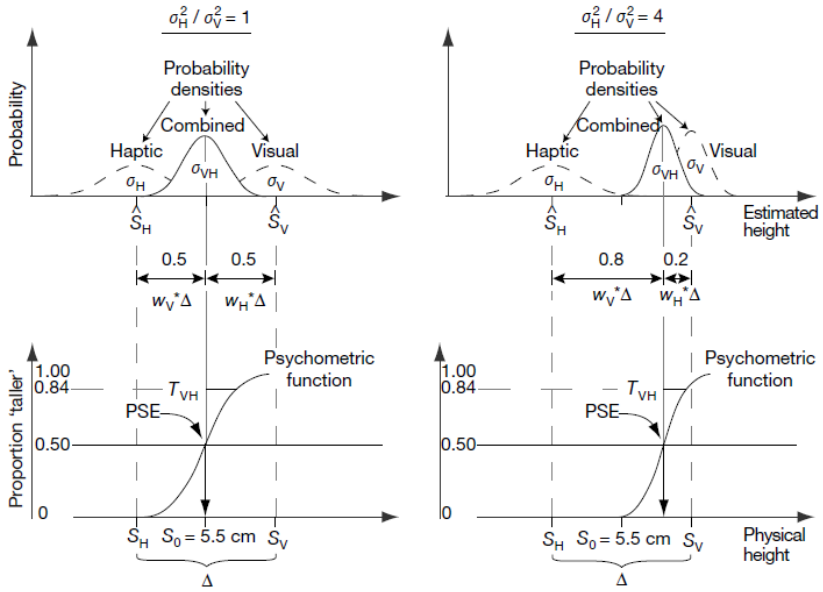

Figure 2.2.1 – Maximum likelihood estimation integration Dashed Gaussians represent probability densities of each modality (haptic and visual sensory information). The thick Gaussian represents the probability density of the combined estimate. On the left panel, both variances are equal and the mean of the combined density is thus equal to the mean of both densities and the variance is divided by two. The psychometric function is the cumulative gaussian with a point of subjective equality (PSE) equal to the average of visual and haptic estimates. On the right panel, the haptic variance is four times bigger than the visual one. The combined density and the psychometric curve are thus shifted towards the visual estimate and the combined variance is equal to 0.8 times the visual variance. [13]

On the figure 2.2.1, the left panel represents the case where both modalities had the same reliability. In this situation, both haptic and visual curve had the same shape and thus the probability density when both modalities were in place was just the average of each probability. However, when disturbing more one modality, its reliability decreased and so the dominance had been given to the other. In the situation of the experiment performed by Ernst & Banks, the haptic variance was four times higher than the visual one. Thus, the combined estimated was dominated by the visual input.

Bayesian approach : Bayesian integration

The Bayesian theory of the optimal cue integration allows considering prior experience acquired through development and learning of the distribution of sensory information. The use of a Bayesian strategy requires a representation of the prior distribution and of the level of uncertainty in the sensory feedback. [10, 16]

Taking back the previous example of $X \sim \mathcal{N}(\mu, \sigma_X^2)$ and $Y \sim \mathcal{N}(\mu, \sigma_Y^2)$ two sensory

signals from different sources. The Bayes rule gives:

$$\begin{aligned} P(\mu \mid X, Y) &\propto P(\mu)P(X, Y \mid \mu) \\ &= P(\mu)P(X \mid \mu)P(Y \mid \mu) \end{aligned}$$

The estimates minimizing the error is then : $\hat{\mu} = \alpha X + (1-\alpha)Y$ With $\alpha = \dfrac{1/\sigma_X^2}{1/\sigma_Y^2 + 1/\sigma_X^2}$, exactly the same as for the frequentist approach.

In the 2004 paper of Körding & Wolpert on Bayesian integration in sensorimotor learning [12] an experiment was conducted in which they controlled the statistical variations of a new sensorimotor task and manipulated the uncertainty of the sensory feedback (Figure 2.2.2).

The experiment consisted of a reaching task without any vision of the hand location. Participants were asked to go as close as possible to the target, with as visual feedback of the finger position only provided briefly, midway to the movement. The reliability of the feedback has been modulated on each trial. There were four conditions : The visual feedback was provided clearly (σ_0), blurred to increase the uncertainty in a middle way (σ_M) or in a large way (σ_L), or even not provided at all (σ_∞). Moreover, during each trial, the visual feedback was shifted laterally relative to the true finger location. This shift was randomly drawn from a prior Gaussian distribution with a mean of 1 cm and a standard deviation of 0.5 cm.
Thanks to this experiment, they observed that the more uncertainty participants had on the feedback, the more their estimate tended to be close to the prior function.

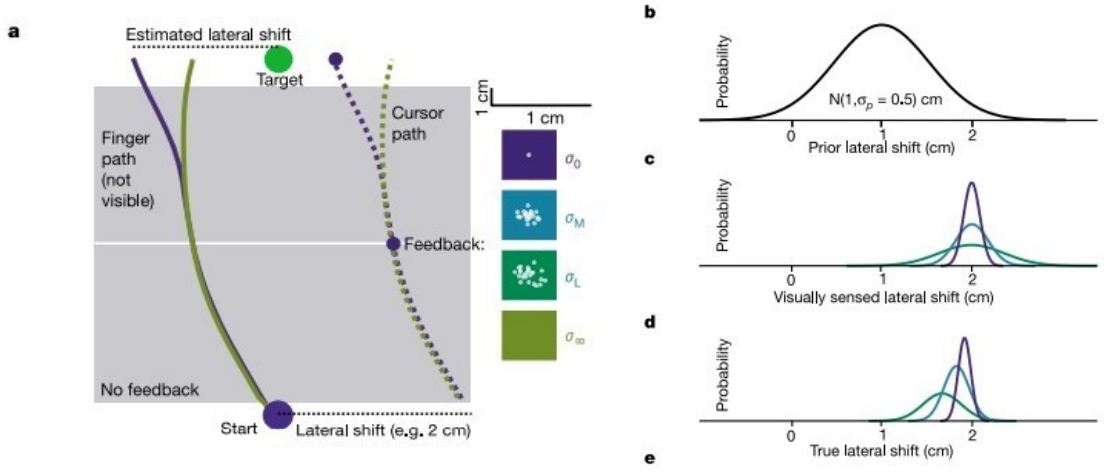

Figure 2.2.2 – Bayesian integration **a.**Experiment protocol of the Körding & Wolpert experiment. Finger paths illustrate typical trajectories when the lateral visual shift was 2 cm. Purple lines represent the situation in which clear visual feedback was provided, and green ones the situation when no visual feedback was provided. **b.**Prior distribution of lateral visual shifts. **c.**Probability distribution of visually experienced shifts for situations where the visual feedback was provided clearly or blurry (colors follow the legend of **a.**. **d.**Estimate of the shift for an optimal Bayesian observer.

What Körding & Wolpert showed in this paper is that people are able to learn the prior function in order to integrate it in their internal model. Indeed, the lower the reliability of the visual feedback was, the more confidence participants had in their expectation of the upcoming perturbation (prior probabilities).

So far, the theory of cue combination has been explored and its main idea is that two cues presented simultaneously will have an influence on each other. Because of this influence, the precision of the combined estimate is always better than both individual precision. Indeed, one cue can be used to reduce the uncertainty of the other.

However, although combining two signals from the same source does indeed improve the precision of environmental perception, combining two signals from different events reduces the correspondence between the perception and the environment and it would lead to behavior that is not well adapted to the environment. [17, 18]
This raises what is commonly referred to as the causal inference that formalize and address the problem of integrate or segregate two signals.

2.3 Causal inference

When several sensory signals reach the controller, the latter must determine whether or not these signals come from the same source. This decision is firstly based on top-down congruency expectations. For example, if you are conversing with a single person, you will tend to integrate the auditory signals you hear and the movements of his lips. On the other hand, if you are in a crowded place, you will not trust what you hear and you will give more importance to what you see. This is what is called prior common source.[19]
Secondly, spatial and/or temporal disparities between sensory signals will also determine whether signals should be integrated or segregated. This is referred to bottom-up sensory congruency cues because it is realized at the moment of sensory input during state estimation. [20][21]

According to Shams & Al (2010) [22], every system that estimates unobserved variables based on observed variables makes inference. For the causal inference theory, the nervous system has to interpret cues in terms of their causes.

Bayesian Causal Inference

Hierarchical Bayesian Causal Inference gives a rational strategy to balance between information integration and segregation in cognition and perception. [23]

For example, let's take an auditory signal (x_a : a voice) and a visual signal (x_v : a moving mouth). (See figure 2.3.2) These signals can either come from the same source ($s = s_a = s_v$: Speaker one) or from two different sources (s_a : Ventriloquist and s_v : puppet). The probability of these two signals coming from the same source (C=1) can be described using Bayes rule and posterior probability : [22, 21]

$$P(C = 1|x_a, x_v) = \frac{P(x_a, x_v|C = 1)P(C = 1)}{P(x_a, x_v)} \tag{2.3.1}$$

With $P(C = 1)$ the expectation of a common cause before receiving sensory input and $P(x_a, x_v|C = 1)$ the probability of the sensory inputs to have been generated from a common source.

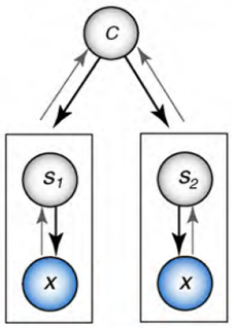

Figure 2.3.1 – Hierarchical Causal Inference Generative model including two or more causal structures (boxes). The inference process (gray arrows) determines the probability of each causal structure. White nodes represent the hidden variables and blue nodes the observed variables.[22]

From this equation, the optimal estimate of the source S_a can be expressed as a non-linear function of sensory cues and composed of the estimate from each structure weighted by their own probability :

$$\hat{S}_a = P(C = 1|x_a, x_v|)\hat{S}_{a,C=1} + P(C = 2|x_a, x_v|)\hat{S}_{a,C=2} \tag{2.3.2}$$

Causal inference in motor action

It has been shown that causal inference also plays a role in motor action and adaptation. [22, 20].

Indeed, the Bayesian causal inference model calculates the probability of an error being relevant to the motor plant and derives an optimal strategy to make the most accurate movement.
When facing perturbations, the nervous system integrates error information and uses it in order to improve future motor tasks. Nowadays, typical models assume that the adaptation to a disturbance by the nervous system is linear and proportional to the errors [20].

However, they did not take into account the errors caused by a disturbance exterior to the motor system (caused by the stochasticity of the world).

An example has been shown by Wei & Al (2009) [20] where they asked participants to make reaching movement in virtual reality while they perturbed the visual feedback. Then they used a Bayesian model to analyze the relevance of the visual feedback and estimates if it has to be used for adaptation or if it has to be ignored :

$$P(relevant|x_v, x_p) = \frac{P(x_v, x_p|relevant)P(relevant)}{P(x_v, x_p)} \tag{2.3.3}$$

$$P(x_v, x_p) = P(relevant)p(x_v, x_p|relevant) + P(irrelevant)P(x_v, x_p|irrelevant) \tag{2.3.4}$$

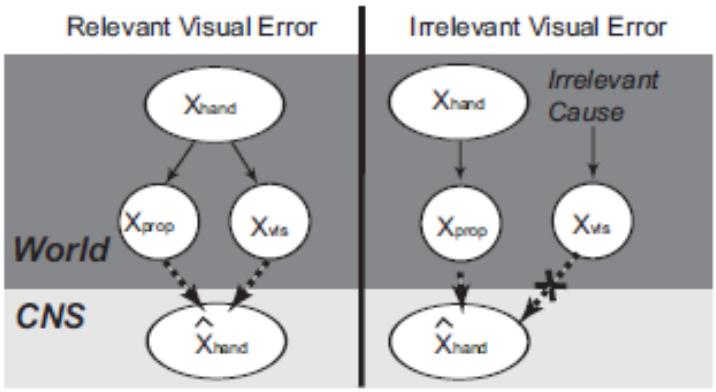

Figure 2.3.2 – Relevance estimation. If error is relevant, both visual and proprioceptive cues are used to estimate the hand position. If the error is irrelevant, only proprioceptive information is taken into account for the estimation of the hand position. The final estimate of the hand position is the average of both estimations weighted by the probability of each case to occur given both sensory modalities.[20]

This analysis leads them to the same conclusion as for auditory and visual cues interaction which declare that the relation between the motor correction and the error size is a non-linear function. Indeed, if the error is much bigger compared to the variability of motor behavior, the CNS does not attribute this error to the motor system but to external factors such as the experimenter. The largest correction is thus linked to the largest error that is still attributed to the motor system.

2.4 Multisensory integration in motor control

As explained at the beginning of this work, in order to perform a voluntary movement, we need the most accurate estimation of the position of our arm. To do so, two sensory signals will be integrated : the visual and the proprioceptive signals. Proprioception is

the sense of body position perceptible at the conscious but also at the unconscious level. It includes information about the position and velocity of the limb based on changes of muscle length detected in the muscle, skin and joints of the body. It also tells the brain what forces are acting upon the body. [24]

A lot of studies have analyzed the way visual and proprioceptive signals are combined to estimate the arm position. [14, 25, 26, 16] These studies raised two important basic aspects of the combination of proprioceptive and visual feedback. Firstly, while visual feedback is conditional (blind people have correct motor skills), proprioceptive feedback is always present as it comes directly from muscle receptors. Secondly, visual feedback is accurate and slow and proprioceptive feedback is fast but less precise. There is thus a form of trade-off between speed and accuracy. [5, 27]

A key aspect of multisensory integration is to minimize the estimation variance. Under this principle, because of the high accuracy of visual information, vision often has a dominant role in the combined sensory signal given to the CNS.
However, one aspect that has not been taken into account in the static study of sensory integration is the importance of the delays of the different sensory signals.

Dynamic multisensory integration

Sensory delays are present in different parts of the sensorimotor control system from the reception of the sensory information to the motor output passing by the transmission of the sensory information along nerve fibers, the computation of the responses by processing this information and the feedback transmission. [28].
Some studies on perceptual decisions have shown that when multiple sensory inputs are involved, the optimal integration of evidence, whose reliability stays constant during a single trial, is done by first looking at the reliability-weighting sum of evidence and then integrating it across time. [29, 30]. However this is no more possible when the reliability changes over time within a single trial.

The problem of the impact of time on sensory integration is all the more important in the context of motor control. Indeed, the information that has to pass through the CNS when we are dealing with a voluntary movement implies consequential delays. As illustrated on the figure 2.4.1, it takes around 60 ms for the limb afferent feedback to reach the controller (R2) and around 90 ms for the visual feedback.

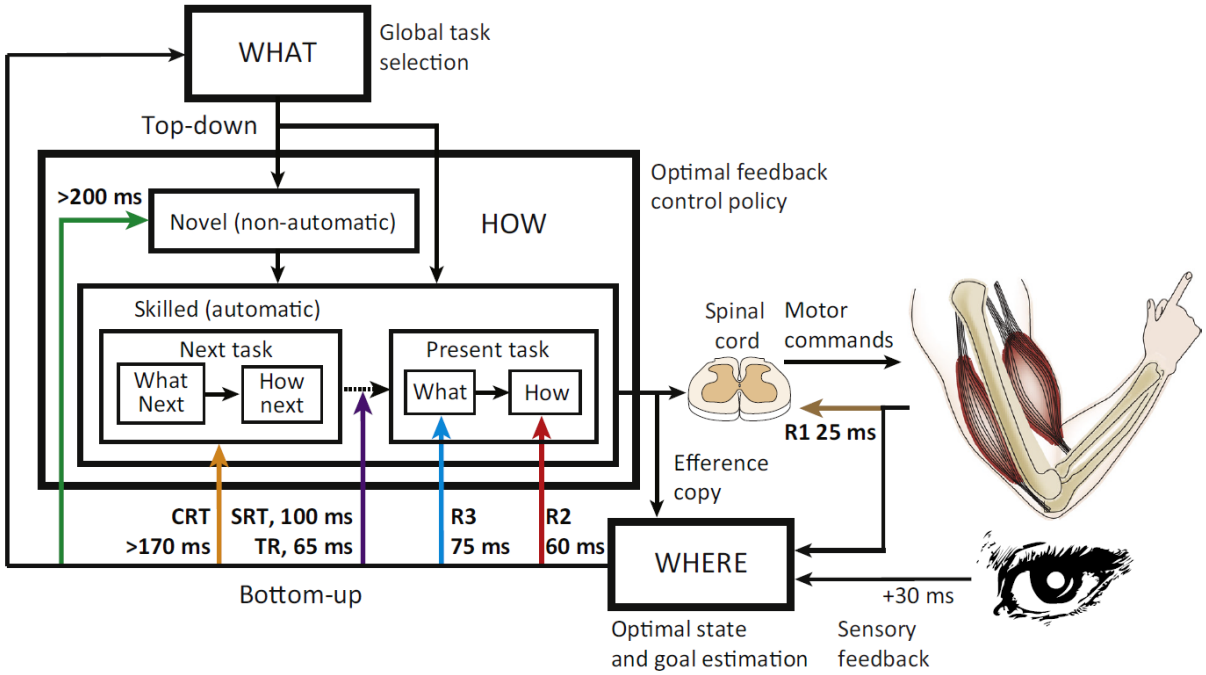

Figure 2.4.1 – Expansion of Optimal Feedback Control policy. Highlighting of the bottom-up sensory feedback useful in motor control and task selection. The times and arrows reflect the feedback from limb afferent signals. The influence of visual feedback is similar but delayed by around 30 ms corresponding to the retinal processing. R1, R2 and R3 represent the initial epochs of muscle stretch response with R1 corresponding to the stretch response in the spinal cord and occurring below the level of control policy (not goal-directed), R2 the online control of the limb and R3 the online control of the goal. The SRT is the Simple Reaction Time, the CRT the Choice Reaction Time and TR the triggered reaction. [5]

In their study Crevecoeur & al(2016) [11] showed a biomechanical model in order to formulate the problem of optimal estimation and control while integrating vision and proprioception undergoing perturbations in presence of temporal delays (δt_p for proprioceptive delay and δt_v for visual delay).(Figure 2.4.2)

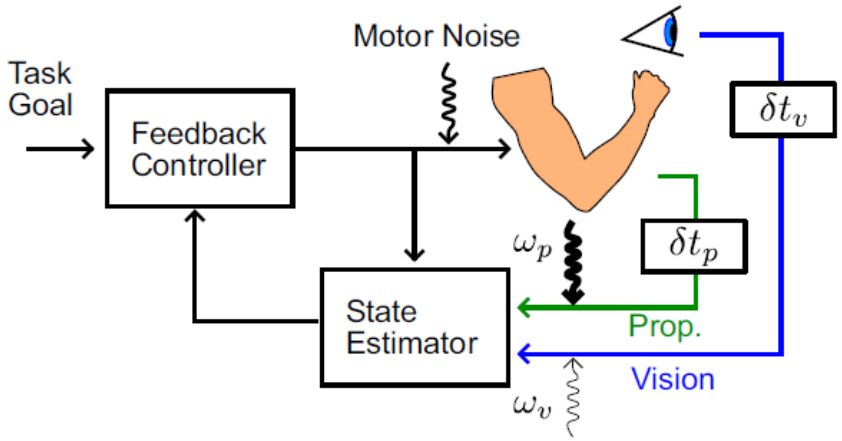

Figure 2.4.2 – Dynamic Bayesian Model Real-time feedback controller based on state estimation. The blue arrow represents the visual sensory input and the green one represents the proprioceptive sensory input. Each feedback has its own delay (δt_v and δt_p) and its own noise (ω_v and ω_p) [11]

This model called dynamic Bayesian model is a state estimation model that accounts for asynchronous delays between sensory cues. To do so they have integrated, into the state estimation assumed in the LQG control, a forward model about the plant that could be used to estimate the current state of the limb from delayed sensory feedback from multiple cue modalities.

Thanks to this model, they have shown that the estimation of the hand motion using dynamic Bayesian model relies almost only on limb afferent feedback. In other words, when there is no visual feedback while correcting for a mechanical perturbation, it does not affect the correction itself but the variation of the endpoint will increase.
This is explained by accumulation of noise over the delay period that makes visual input less accurate for the estimation of the present state. The proprioceptive delay is shorter then this modality is dominant.

Another study by Kasuga & al. (2022) [27] went further and analyzed how proprioceptive and visual feedback are integrated together during online control. To do so, they performed various experiments where visual and/or mechanical disturbances were present. Their main observation was that indeed visual feedback does not increase the size of muscle response while undergoing a mechanical disturbance but do decrease the variability in lateral hand position. However, when there is a visual disturbance in the opposite direction of the mechanical disturbance, visual feedback becomes substantially influential. The key assumption made during their study was that both sensory feedback updated separate estimate of the position with the aim of reaching the target. They showed that the motor system is able to choose to integrate visual and proprioceptive feedback in a combined or separate way depending on the task to be performed and the perturbation encountered.

This possibility of dissociation between the integration of the visual and proprioceptive signals during motor control refers to the theory of causal inference explained in the previous section. This raises the question whether multisensory integration may vary dependent on the assumption made about hand-cursor motion.

2.5 Experiment

This study attempted to answer this question by conducting two experiments in different contexts but with the same visual and mechanical disturbances.
More precisely, this study consisted of comparing the performance of a task in which the visual feedback provided could be deviated from the true participants' hand location. In one context, the participants were aware of this visual perturbation, whereas in a second context they were not.

Concretely the aim of this thesis is to investigate the contribution of visual and proprioceptive feedback on movement control and adaptation. Specifically, we want to study whether this contribution is modulated by participants' awareness of whether or not the provided visual feedback is congruent with their true hand location.

2.6 Potential predictions

Following the theory of Kasuga & al. (2022) [27] two integration scenarios are possible.
On one hand, the hand and the cursor position could be integrated together as one same source of information. In this case, both sensory feedback would be integrated together driving a weighted average of the cursor and hand position to the target.
On the other hand, both visual and proprioceptive feedback should be dissociated and integrated separately. In this situation, vision would have a larger impact on movement correction if participants believe that it represents accurately their hand location, whereas visual influence would be reduced if participants are aware of the discrepancy between their felt hand position and the visual feedback provided.

Given the causal inference theory (Section 2.3), it is expected to face the second prediction and to see a segregation of the sensory information during the instruction where participants are aware of the possible deviation of the visual feedback from the true hand location.

Chapter 3

Material and methods

3.1 Participants

Sixteen healthy right-handed participants aged 22 to 27 years old (7 females) took part in this study. All of them had normal or corrected-to-normal vision. Each of them participated in both experiments. The experiments were performed in accordance with the rules of the university ethics committee and all participants gave written informed consent to participate in the study.

3.2 Task Protocol

The experiments were performed using a KINARM Endpoint robotic device (BKIN Technologies, Kingston, Canada). The participants were sitting on an height-adjustable chair (figure 3.2.1.E) with their foreheads rested against the frame of the robot (figure 3.2.1.C). Their hand holding the robotic handle (figure 3.2.1.D) was concealed below a screen. A virtual reality system displayed the experiment protocols and the hand was represented by a hand-aligned cursor. The visual targets displayed by the monitor on the top of the set-up (figure 3.2.1.A) are reflected into the movement plane using a mirror(figure 3.2.1.B) which is placed above the shutters that close above the handle and the hand. Experiments were designed using Matlab toolboxes Simulink and Stateflow (Matlab 2015, Mathworks Inc. Natrick Ma,USA).

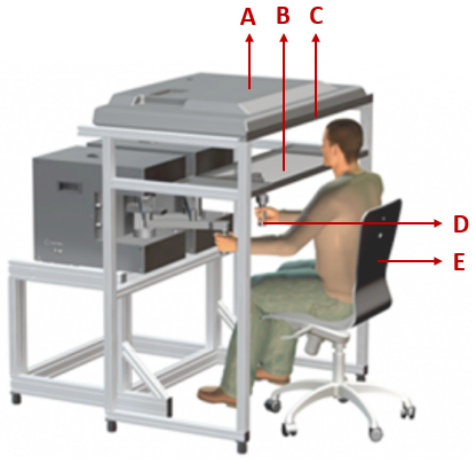

Figure 3.2.1 – Illustration of the KINARM Endpoint robotic device (BKIN Technologies, Kingston, Canada) used to perform the different experiments. **A**.Monitor displaying the computer inputs. **B**.Semi-transparent mirror. **C**.Cushion for participants to rest their forehead **D**.Robot right handle allowing horizontal plane movements. **E**.height-adjustable chair [31]

Participants were asked to perform a total of 680 reaching movements of 15 cm spread over two experiments with their right hand while holding on to the right handle of the robotic device. A start target (blue disc 12 mm diameter) was displayed 5 cm from the body and a goal target (blue circle 24 mm diameter) was displayed 15 cm further away from the body (Figure 3.2.2).

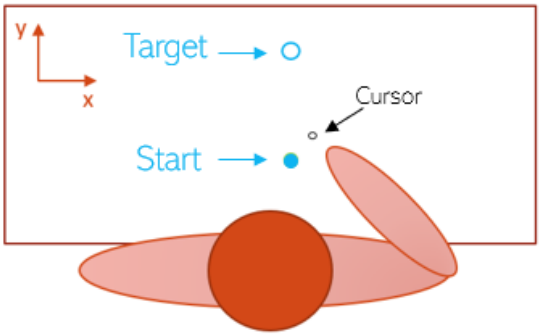

Figure 3.2.2 – Workspace of the Experiment.A virtual reality screen obstructed the participants' view of their hand. They were asked to make a reaching movement with a hand-aligned cursor from a start 5 cm in front of them to a final target 15 cm away.

At the beginning of each movement, participants were instructed to move to the starting position (which turned green at the moment they were in place) and remain there until they received a go signal (Figure 3.2.5(a).A and figure 3.2.5(b).A).
This go signal, represented by the filling in of the target circle, occurred after a random delay drawn from a uniform distribution between 2 and 4 seconds (Figure 3.2.5(a).B and figure 3.2.5(b).B).
As soon as the go signal was given, participants were instructed to move quickly towards the target and hold their hand into it 1 second. The movement had to be performed at a

speed between 0.5 m/s and 0.8 m/s (Figure 3.2.5(a).C and figure 3.2.5(b).C).
During these reaching movements, different types of perturbations could occur simultaneously. Firstly, the participants could pass through a positive or negative force field Clockwise (CW) or Counter-Clockwise (CCW)). These force fields, also called orthogonal velocity-dependent force fields, were applied to the handle of the robot as a load of $\pm 13N$ proportional to the forward velocity (Figure 3.2.3(a)).

$$\begin{bmatrix} F_x \\ F_y \end{bmatrix} = \begin{bmatrix} 0 & L \\ 0 & 0 \end{bmatrix} \begin{bmatrix} \dot{x} \\ \dot{y} \end{bmatrix} \tag{3.2.1}$$

Secondly, a scaling of the lateral deviation of the cursor by a factor of .3, 1, or 1.7 could be applied.(Figure 3.2.3(b)).

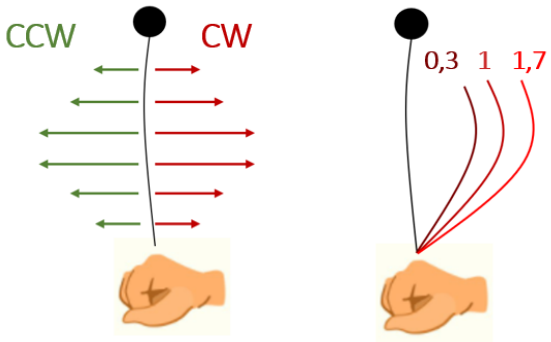

(a) Force field disturbance (b) Visual Gain disturbance

Figure 3.2.3 – While performing the reaching movements, the participants could encounter two types of perturbations. First, they could pass through a positive or negative force field (Clockwise (CW) or Counter-clockwise (CCW)). Secondly, a scaling of the lateral deviation of the cursor by a factor of .3, 1, or 1.7 could be applied. All the results presented in this work will follow the color logic shown here, i.e. shades of red for all CW force field movements and shades of green for CCW force field movements.

After staying 1 second in the final target, three types of feedback were possible (Figure 3.2.5(a).D):
First the final target could change to red and the message "Too Fast" would appear on the screen. This meant that the participant had performed the movement with a forward velocity higher than 0.8 m/s. Secondly, it was possible that the target turned green and participants received the message "Target Hit!". This meant that the participant had performed the task correctly. Finally, if the participant had not reached the target correctly or had moved too slowly, the target would turn light blue and the message "Too Slow!" would appear on the screen.
To motivate the participants to do their best and to keep track of the success rate of each

experiment, participants received one point for every correct movement.
Before starting the experiment, each participant performed 10 training movements in order to become familiar with the setup. These training movements were not subject to any perturbation (baseline trials) and were not part of the analyses. Then one entire experiment consisted of 5 blocks of 66 reaching movements with a short break in between to limit the effect of fatigue due to prolonged concentration. Each block was built in a semi-random way : the first and last trials were baselines and there was at least one baseline trial after each trial undergoing a perturbation in order to limit the anticipation of the disturbance by the participant. In total, for each instruction, participants performed 180 baseline trials and 150 movements pertubated. Of these, half experienced a CW force field and half a CCW force field. Also, each visual gain was applied to 50 trials.(See figure 3.2.4)
Eight participants began with the first experiment while the others began with the second one.

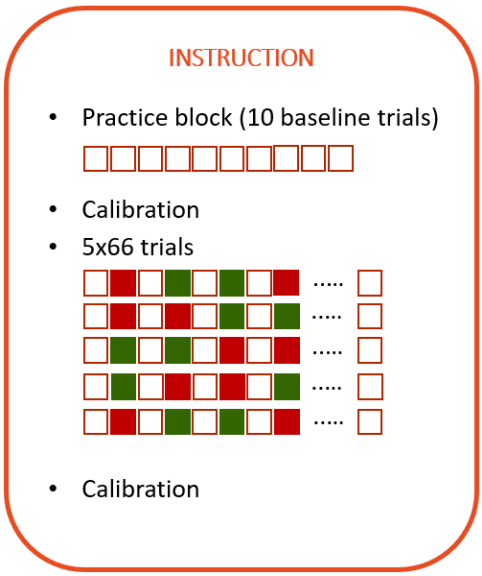

Figure 3.2.4 – Composition of one instruction block. The entire study was composed of two experiments similar in terms of design. First, the participants performed 10 training trials without any perturbation (White squares). Then participants had to perform a first calibration block allowing later on to normalize the muscle signals. After this, the experiment as such began with a sequence of 5 blocks of 66 reaching movements. These blocks were each composed of 30 perturbed: Red squares (CW) or Green squares (CCW) and 36 baseline movements : White squares. The first and last trials, as well as each trial following a disturbance, were baseline trials. Finally, participants had to perform a second calibration block as just before.

Experiment 1 : Instruction to control the cursor

In the first experiment, the participants were asked to place the cursor inside the target without telling them that the cursor could deviate from the true location of their hand. They were told that their hand was represented by the cursor and that during the reaching movement they might encounter a force that they would have to counter. However, they

were not told when or in which direction this force would appear.
The purpose of experiment 1 was to investigate the contribution of visual feedback to movement corrections when it was assumed to be congruent with the true hand position.

Experiment 2 : Instruction to control the hand

In the second experiment, we asked participants to place their hand inside the target while having no direct vision of its actual position. The only visual information available to them was a cursor that they knew was potentially deviating but still controlled by their hand.
In terms of the force field experienced, they had exactly the same information which was the possibility of experiencing a force to be countered but without knowing when or how. The aim of this experiment was to analyze the effect of visual feedback on participants' motor corrections when they were clearly aware that the visual information they received might be false.

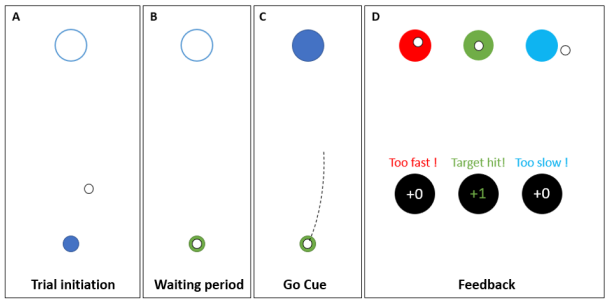

(a) Cursor instruction protocol

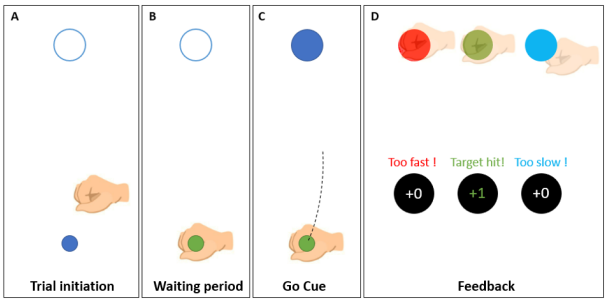

(b) Hand instruction protocol

Figure 3.2.5 – Tasks protocols. The whole experimental work was composed of two experiments that differed by the instructions: To control the cursor(a) and to control the hand (b). Each of them was structured almost the same way. The difference was the instruction given to the participant. One trial was carried out in four stages. **A**: Trial start. *Participants' hand was represented by a white cursor. Start target was blue and final target was empty.* **B**:Participants moved into the start circle. *The start target was green but the final target was still empty.* **C**: Go cue signal. *The final target was filled. Participants had to move rapidly into the final target.* **D**: Feedback. *Upon remaining inside the final target for 1s, participants received a feedback red, green or blue depending on the success of the trial or not. A score zone represented by a black disk with the point was displayed simultaneously.*

3.3 Data collection

During the experiments two kinds of signals were studied : kinematics and electromyography (EMG).

Kinematic signals

The position of the hand was sampled at 1 kHz by the KINARM robot. The velocity and acceleration were numerically computed from these coordinates information using a second-order central-differences algorithm.

EMG signals

The signals of the muscles involved in both experiments were recorded by EMG. Therefore, bipolar surface electrodes (DE-2.1 EMG Sensor, Delsys, Natick MA, USA) were placed on the Pectoralis Major (PEC), shoulder flexor muscle and on the Posterior Deltoid (PD) shoulder extensor muscle of the participants. Two other electrodes were placed on the Triceps Lateralis (TL), elbow extensor muscle and Brachioradialis (BR), elbow flexor muscle. All this was done on skin that had been previously cleaned and lightly abraded with alcohol. In addition, a conductive gel was placed between the electrode and the skin in order to increase signal-to-noise ratio. EMG signals were amplified by a factor of 1k or 10k (depending on the subject) (Bagnoli-8 EMG System, Delsys, Natick MA, USA).

3.4 Data analysis

Preprocessing

All signals were first aligned to movement onset and cut from 200 ms before to 1 second after it using Matlab R2018b (Mathworks 333 Inc. Natick MA, USA).
All kinematic data were digitally low-pass filtered (eighth-order dual-pass Butterworth, 50 Hz).
EMG signals were first digitally bandpass filtered (eighth-order dual-pass Butterworth :[10-400] Hz). Secondly, EMG signals were rectified and finally they have been normalized by dividing them by the average activity during calibration trials in the direction which activates the concerned muscle. These calibration trials consisted of asking the participants to hold their hand in a specific location by counteracting a constant force of 5N applied for a period of 2 seconds. This constant force was applied in 4 different directions to activate the four muscles of interest: Pectoralis Major, Posterior Deltoid,Brachioradialis and Triceps Lateralis. One calibration block was composed of 12 force repetitions (3 in

each direction).

Statistical analysis

Firstly, in terms of kinematic data, three outcome variables were studied: the maximum lateral deviation of the hand relative to baseline movements, the endpoint error relative to the target position and the after-effect.
The first one was extracted by taking the first peak of the lateral deviation for each perturbed trial and then comparing them in terms of trial conditions (Force Field (FF) direction, Visual Gain (VG) and task).
The second one was computed by looking at the lateral endpoint deviation relative to the target position for each trial and comparing them in terms of trial conditions too.
Finally, the third one was measured by taking the first peak of the lateral deviation relative to target X position of baseline trials directly following a perturbation. These values were then also compared in terms of trial conditions.

Secondly, in terms of EMG data, three other outcome variables were studied: the early and late muscle responses and the average baseline activity during movements.
The first two variables were measured by taking the average of the muscle responses of interest in the two time windows concerned.
For the early muscle response, the activity of PEC when the trial was undergoing a CW force field and that of PD when the force field was CCW were taken into account. These muscle responses were averaged over a time window ranging from 100 ms to 300 ms after the movement onset.
For the late EMG activity, the muscle response of PD was taken when the trial was subjected to a CW force field and that of PEC when the force field was CCW. These activities were averaged over a time window of 300 ms to 500 ms after the movement onset.
Third the baseline muscle responses were averaged across instructions for each participants.

Finally, failure rate for each instruction was computed in order to analyze the complexity of each task for participants.
To assess the effect of force-field direction and visual gain on movement corrections, as defined by the measures above, statistical tests were performed for each measurement. The statistical tests used were a Linear Mixed Model (LMM) and paired samples t-tests.[32]

Linear Mixed Model The general matrix form of the model is as follows:

$$Y = X\beta + Zu + \epsilon \tag{3.4.1}$$

The equation 3.4.1 is composed of :

— Y : The outcome variable, also called dependent variable. In this case the outcome variables were : the maximum hand and endpoint lateral deviations, the after-effect, the early and late muscle responses and the maximal forward velocity.

— Xβ : Fixed effects, also called independent variables. In this case fixed effects were the instruction of the trial (Cursor or Hand) and the visual gain of the trial (.3,1,1.7)

— Zu : random intercept terms were defined for each participant.

— ϵ : The residual error term

Every statistical tests were performed separately for CW and CCW force-field trials.
All test returning p-values below .05 were regarded as significant.

Paired-samples t-test Paired-samples t-test were performed on the failure rate and on the baseline muscular activity.

Chapter 4

Results

The aim of this thesis was to study whether the contribution of visual and proprioceptive feedback on movement control and adaptation is modulated by participants' awareness of whether or not the provided visual feedback is congruent with their true hand location. To do so, two experiments were implemented. Both required participants to perform reaching movements while having no vision of their hand and encountering mechanical and visual perturbations. In the first experiment, participants were asked to control the cursor and in the second they were asked to control their hand. The idea was to understand how the problem that the brain has to solve (control the hidden hand instead of the visual cursor) is linked to what it learns from experiencing different types of perturbations.

The hypothesis was that by asking participants to control their hand instead of the cursor, the influence of visual feedback should decrease. Indeed, by informing participants of the unreliability of visual feedback, accordingly to the experiment of Shams & Beierholm (2022) [21], only proprioceptive information should be taken into account for the estimation of the hand position.

In this section, all the obtained results will be presented in details. Firstly, a study of the effect of the various perturbations and instructions will be carried out. To do this, four kinematic variables were extracted: the maximum lateral deviation, the endpoint deviation, the maximum forward velocity and the after effect. Three muscular variables were also extracted: the early and late muscle responses and the baseline activity.
In a second step, a comparison will be made between the behavior of the group of participants who started with the cursor instruction and those who started with the hand instruction. The purpose of this section is to observe whether the first instruction carried out had an influence on the second.

For the first analyses, each variable was studied separately according to the direction of the force field experienced. For all graphs, trials with a CW force field will be shown in

shades of red and trials with a CCW force field will be shown in shades of green. The experiment requiring cursor control will be represented by a full line and the one requiring control of the hidden hand will be represented by a dashed line.
In the second part of analyses, trials carried out by the group of participants who started with the cursor instruction will be represented by a solid line, while those who started with the hand instruction will be represented by a dashed line.

4.1 Analysis of the effects of the instruction and visual gain

4.1.1 Kinematic data

The average kinematic behavior of participants for each instruction and trial type is shown in Figure 4.1.1.
The top-panel shows that the general trajectories for each type of trial were very similar from one instruction to the other. However, the panel B showing the lateral position during the whole trial allows seeing the correction of the movement after mechanical perturbation was higher for the instruction controlling the hand than the one controlling the cursor. Finally, in terms of velocity, the lower panel shows that the correction occurred faster when participants had to control their hand.

The start movement time point was the moment where participants started to move towards the final target. This time has been extracted for each trial thanks to an event marker from the KINARM robot.
The end movement time index was extracted by an approximation of the moment participants had completed their reaching movement towards the final target and were in the stabilization phase waiting for feedback. This approximation has been made by looking to the general behavior across participants.

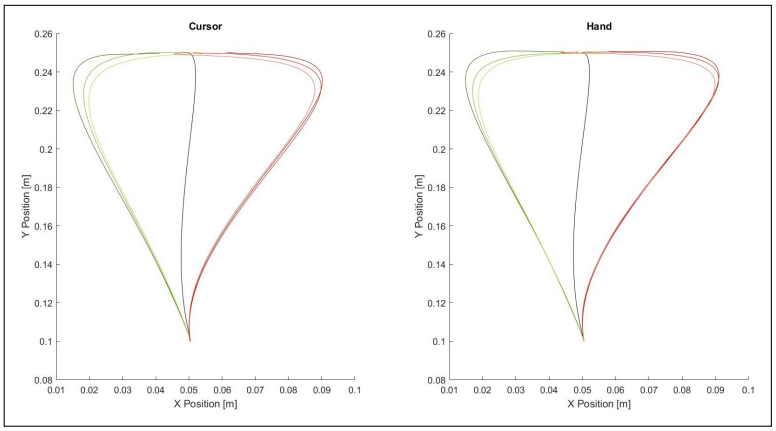

(a) Trajectories

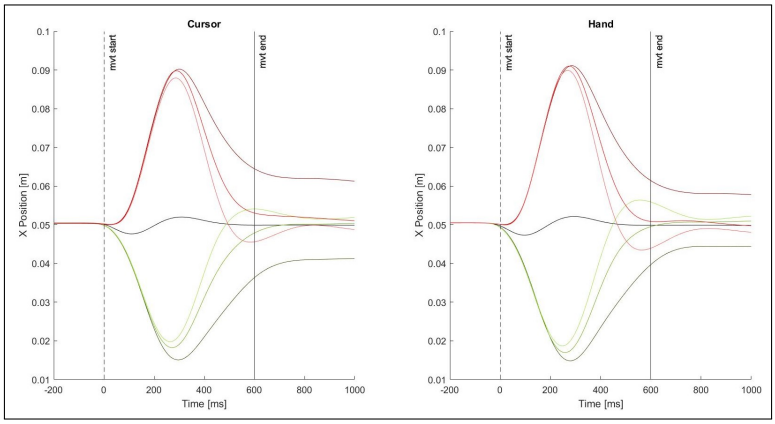

(b) Lateral positions

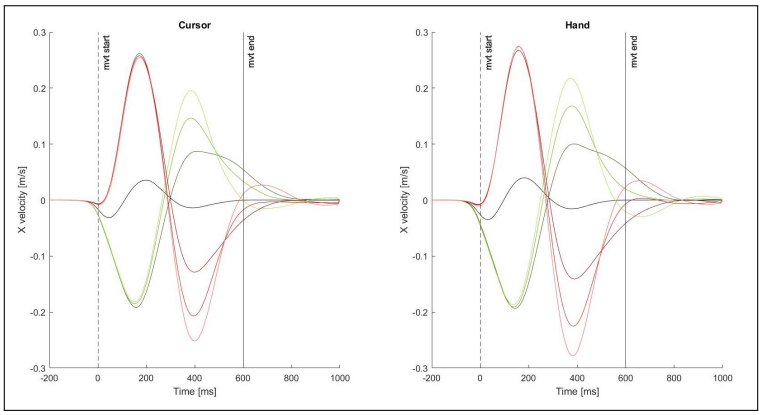

(c) Lateral velocities

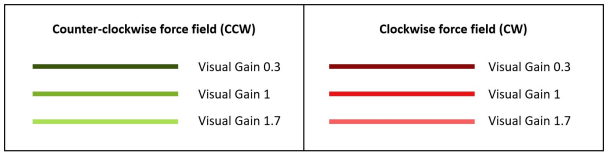

Figure 4.1.1 – Instruction comparison : Kinematic behavior across all participants. Overall mean of trajectories (Top panel), lateral position (Middle panel) and lateral velocities (Bottom panel) across the different combinations of force fields and visual gains. The red lines represent trials with a CW force field and the green ones a CCW force field. The dashed black line indicates the movement onset and the thick one represents the movement offset. Data were aligned on the timing when the hand started moving and were cut from 200ms before this time to 1 second after it. The first column represents the experiment in which participants were asked to control the visual cursor and the second one shows the experiment where they had to control their hand.

Maximum lateral deviation

The first studied aspect was the maximum lateral deviation of the hand trajectory as a function of the visual perturbation for each instruction. This variable has been computed by taking the maximum of the absolute difference between target X coordinate and the hand lateral position for each trial. An average by trial condition was then made and plotted in figure 4.1.2.

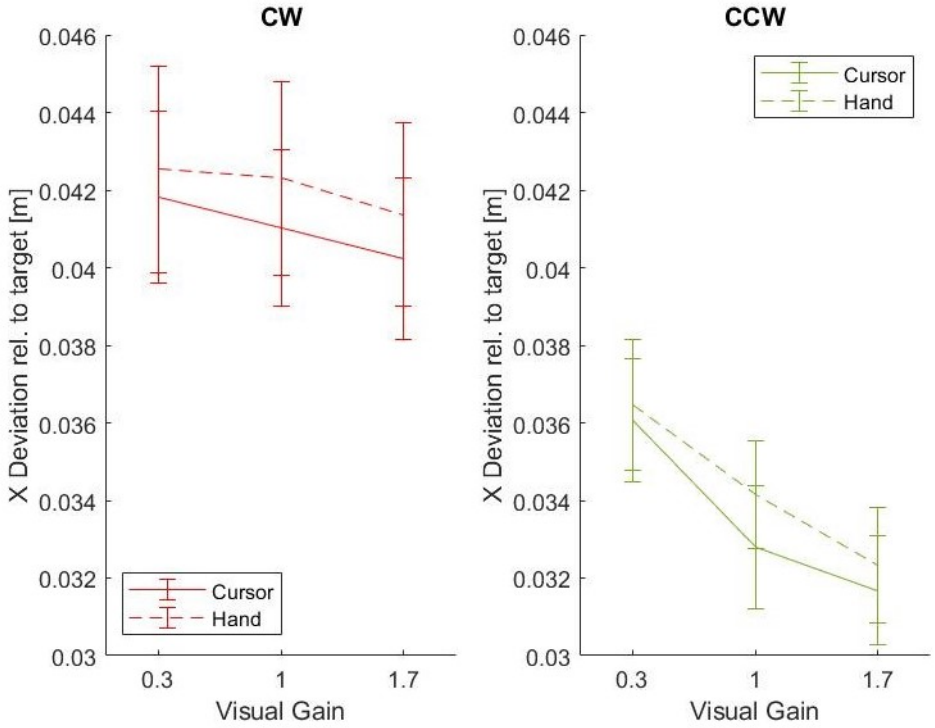

Figure 4.1.2 – Instruction comparison : Maximum lateral deviation relative to the target position. Average maximum lateral deviation relative to the target position for each force field direction in each instruction as a function of visual gain. Each line indicates the across-participants average in each trial type and the standard error of the mean (SME) is shown with the vertical lines. The absolute value of the deviation relative to the target x-position had been taken. Dashed lines represent the experiment where participants had to control their hand while the thick ones represent experiment where participants controlled the cursor.

We observed a significant decrease of maximum hand deviation with increasing visual gain for both force-field directions (CW: slope = -.001, t(2396) = -2.08, p = .04, CI = [-.002,-6.39e-05]; CCW: slope = -.003, t(2396) = -8.07, p = 1.09e-15, CI = [-.0039 ; -.0023]). However, there was no significant effect of the instruction on the maximum hand deviation during perturbations (CW: slope = -.0008, t(2396) = .89, p = .37, CI = [-.0009,.0025]; CCW: slope = -.0006, t(2396) = 1, p = .32, CI = [-.0006 ; .0019]) nor an interaction between instruction and visual gain(CW: slope = -.0003, t(2396) = .35, p = .73, CI = [-.0012,.0017]; CCW: slope = -.0001, t(2396) = .29, p = .77, CI = [-.0009 ; .0012]).

Endpoint deviation

The second effect observed was the endpoint error as a function of the visual gain for each instruction. To do this quantitatively, the endpoint lateral deviation of each trial was computed by taking the average difference between target X coordinate and the lateral position over a time window of 100 ms around an approximate average time of the end of the trial (600 ms). For this analysis, the sign of the endpoint deviation for CCW trial was changed such that for all trials, a greater deviation reflects a bigger endpoint error. Figure 4.1.3 shows the average end point deviation across trial conditions.

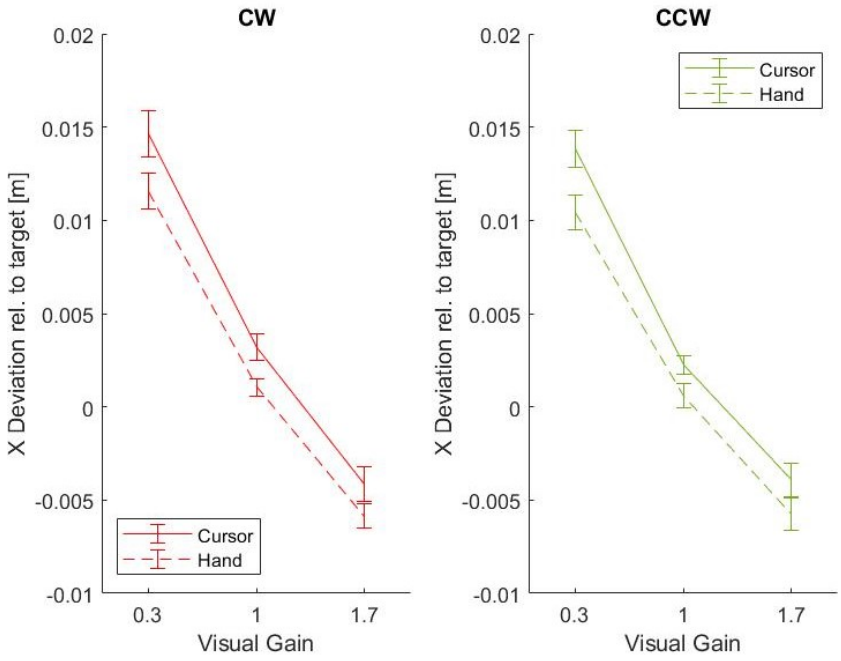

Figure 4.1.3 – Instruction comparison : Endpoint deviation relative to the target position. Average endpoint deviation relative to the target position for each force field direction in each instruction as a function of the visual gain. For this analysis, the sign of the lateral deviation for CCW trials has been changed such that for all trials, a positive deviation represents a bigger distance relative to target position. Each line indicates the across-participants average in each trial types and the standard error of the mean (SME) is shown with the vertical lines. The endpoint error for each trial was computed as the average position over a time window of 100ms centered on 600ms after the movement onset. Color-coding and linestyle follow the same convention as in figure 4.1.2.

We observed a significant decrease of endpoint error with increasing visual gain for both force-field directions (CW: slope = -.003, t(2396) = -4.68, p = 2.96e-02, CI = [-.0047,-.0019]; CCW: slope = -.003, t(2396) = -5.93, p = 3.46e-09, CI = [-.0045 ; -.0023]). There was also a significant decrease of the endpoint error when participants were asked to control the hidden hand instead of the cursor. (CW: slope = -.013, t(2396) = -30.99, p = 1.06e-177, CI = [-.0014,-0.0126]; CCW: slope = -.013, t(2396) = -35.79 , p = 4.07e-225, CI = [-.013 ; -.012]). Finally, for CCW trials, we observed a significant interaction between the task instruction and the visual gain but no significant interaction for CW trials (CW:

slope = .0009, t(2396) = 1.63, p = .10, CI = [-.0002,.0022]; CCW: slope = .001, t(2396) = 2.26, p = .02, CI = [.0001 ; .0021]).

Maximum forward velocity

The third kinematic variable analyzed was the forward velocity and more precisely the average maximum forward velocity as a function of the visual gain. This value was computed by taking the first peak of the forward velocity for each trial and by averaging it across participants and trial conditions. Figure 4.1.4 represents this average maximum forward velocity for each force-field direction.

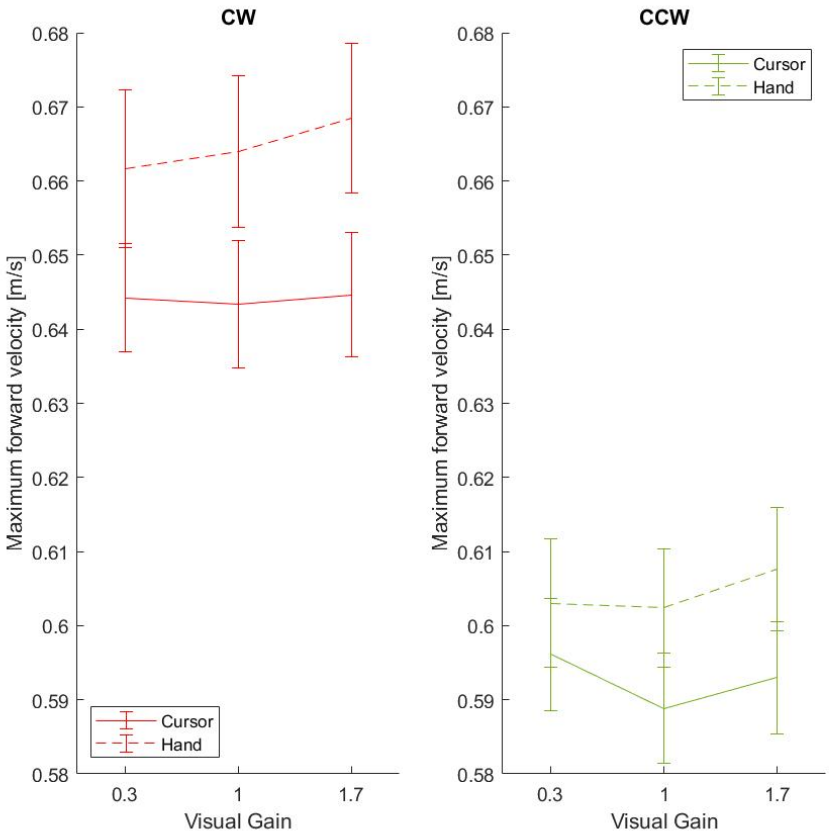

Figure 4.1.4 – Instruction comparison : Maximum forward velocity. Average maximum forward velocity for each force field direction in each instruction as a function of visual gain. Each line indicates the across-participants average in each trial types and the standard error of the mean (SME) is shown with the vertical lines. The maximum forward velocity for each trial was computed by taking the first peak of forward velocity for each trial and then taking the average across trial conditions. Color-coding and linestyle follow the same convention as in figure 4.1.2.

We observed a significant increase of forward velocity when participants were asked to control their hidden hand instead of the visual cursor during CW experiments (CW: slope = .016, t(2396) = 2.63, p = .0085, CI = [.004,.028]; CCW: slope = .006, t(2396) = 1.07, p = .28, CI = [-.005,.02]). However, there was no effect of the visual gain on the forward

velocity (CW: slope = .0003, t(2396) = .08, p = .94, CI = [-.007,.008]; CCW: slope = -.002, t(2396) = -.64, p = .52, CI = [-.009,.005]) nor any interaction between the instruction and the visual gain (CW: slope = .004, t(2396) = .86, p = .39, CI = [-.006,.01]; CCW: slope = .006, t(2396) = 1.11, p = .26, CI = [-.004,.015]).

After effect

The last kinematic aspect studied was the after effect. This variable indicates how much the sensorimotor system has retained from the perturbation experienced during the previous movement and is linked to the idea that the brain learns an internal model of the movement and environmental dynamics has explained in the section 2.1[33].This variable as been extracted by taking the trajectories of baseline trials immediately following a perturbed trial and sorting them by type of disturbance experienced in this previous trial. An average was then taken by force field direction. Additionally, the maximum deviation relative to the target x-position for each instruction and force field direction was extracted to compare the different conditions.(Figure 4.1.5)

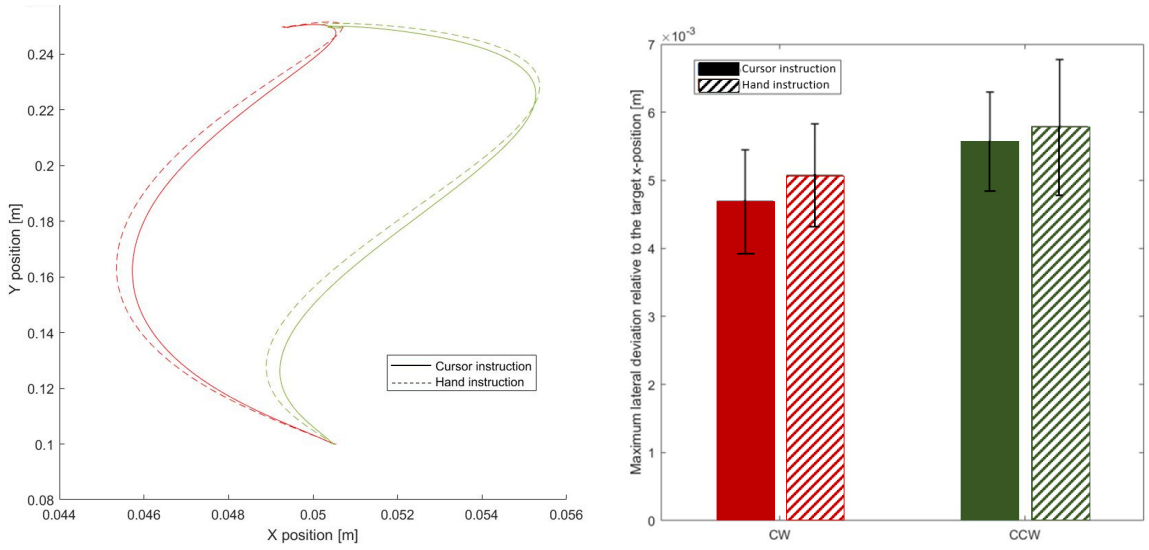

(a) Hand trajectories

(b) Maximum deviation

Figure 4.1.5 – Instruction comparison : After effect **(a):** Across-participants average hand trajectories during baseline trials immediately following a perturbed trial for each instruction. **(b):** Comparison of the across-participants average maximum lateral deviation relative to the target x-position during baseline trials immediately following a perturbed trial for each force-field direction and each instruction. The vertical bars represent the standard error (SME) and the color-coding and linestyle follow the same convention as in figure 4.1.2.

There was no significant effect of the instruction on the after effect for both force-field directions (CW: p-Value = .723, t(30) = -.36, SD = .003, CI = [-.003,.002] ; CCW: p-Value = .856, t(30) = -.18, SD = .003, CI = [-.003,.002]).

4.1.2 EMG data

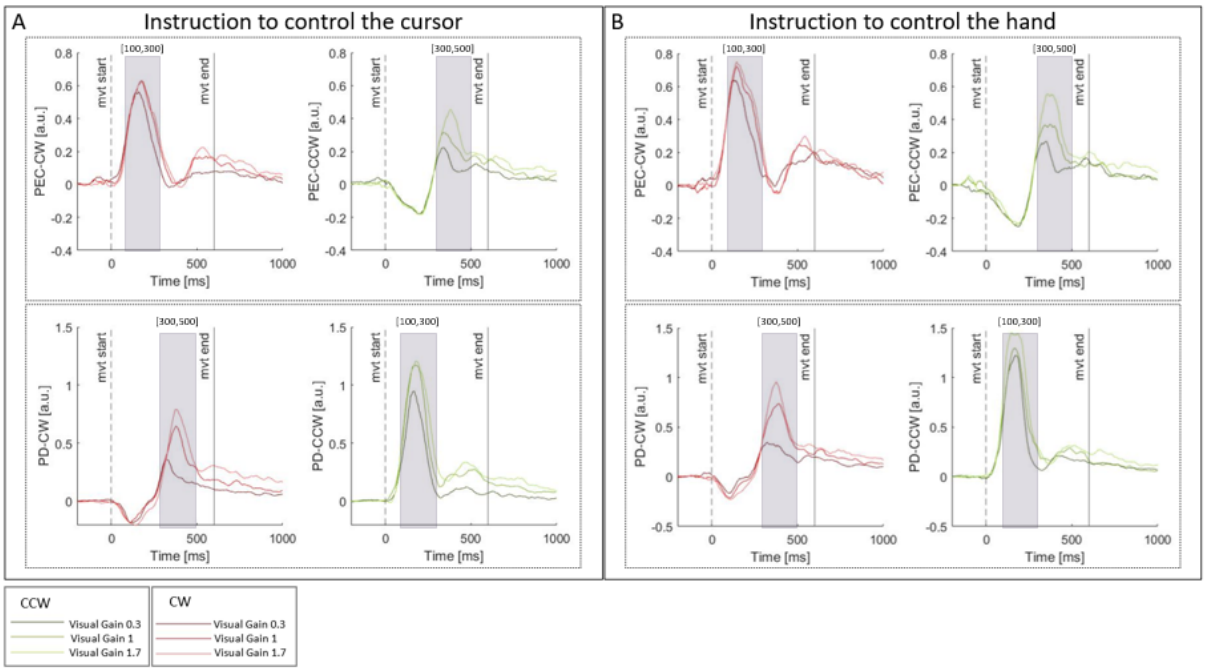

Figure 4.1.6 – Instruction comparison : Muscular behavior across all participants. **A**: Muscular activity during the experiment where participants had to control the cursor. **B**: Muscular activity during the experiment where participants controlled the hand.
First row: Across-participants average of EMG signals of the pectoralis major (PEC) when participants faced CW(red) and CCW(green) force field direction for each visual gain. Second row: Across-participants average of EMG signals of the posterior deltoid (PD) when participants faced CW (red) and CCW (green) force field direction for each visual gain. All the EMG data were preprocessed as explained in the section 3.4. The average activity measured during baseline trials was subtracted from each condition mean represented here and a moving average over a sliding window of 50 ms was used to plot the data.

The average muscular behavior of participants for each instruction and trial type is shown in Figure 4.1.6. The average activity measured during baseline trials has been subtracted from each condition mean in order to better see the scaling across trial conditions.
The first row represents the across-participants activity of the Pectoralis Major in every trial conditions and the second row represents the across-participants muscular response of the Posterior Deltoid in every condition. These signals were plotted by taking the moving average across participants over a sliding window of 50ms.
In order to analyze in more detail the muscular behavior in relation to the different trial conditions experienced by the participants, a time average was performed on the muscle signals.
From this, two variables were extracted: The early and the late muscular responses. The first one was computed by taking the average over a time window from 100 ms to 300 ms after movement onset of the muscular activity of the PD during CCW trials and of the PEC during CW trials. The second one was computed by taking the average over a time window from 300 ms to 500 ms after movement onset of the muscular activity of the PEC

during CCW trials and of the PD during CW trials.

Early muscular response

The first aspect that was studied was the early muscular response. This variable has been computed by averaging the muscle activity subtracted by the average baseline activity of the PEC during trials against CW force field and of the PD during trials against a CCW force field over a time window ranging from 100ms to 300ms after the movement onset. (See figure 4.1.6) Then the mean across trial conditions was computed and plot on the figure 4.1.7.

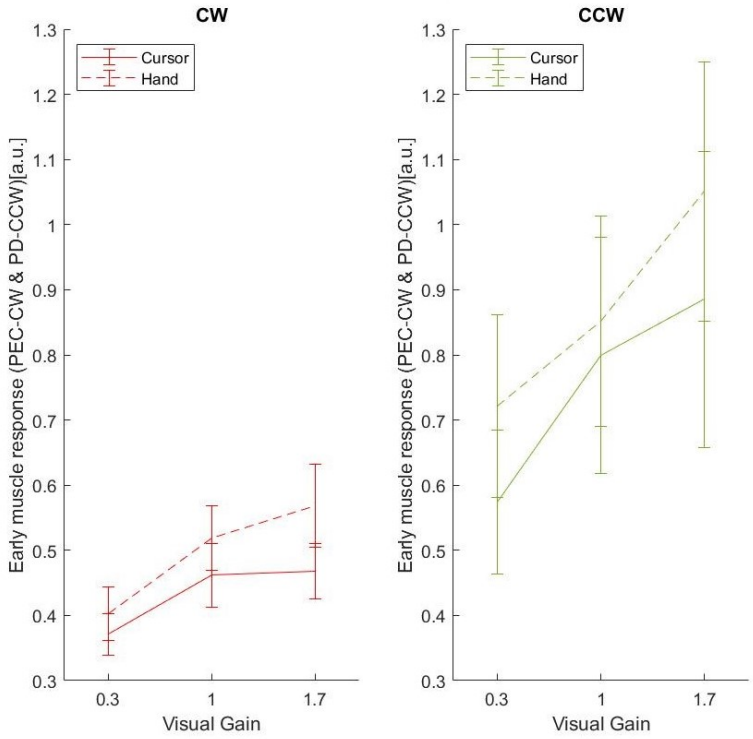

Figure 4.1.7 – Instruction comparison : Early muscular response across all participants. Average early EMG response for each force field direction as a function of visual gain. Each line indicates the across-participants average in each trial types and the standard error of the means (SME) are shown with the vertical lines. Color-coding and linestyle follow the same convention as in figure 4.1.2.

For both force-field directions, we observed an increase of early muscle responses with the size of the visual gain (CW: slope = .093, t(2396) = 3.15, p = 1.66e-3, CI = [.035,.152]; CCW: slope = .22, t(2396) = 4.48, p = 7.98e-6, CI = [.126,.324]). Further, muscle responses were significantly larger in the hand compared to the cursor instruction (CW: slope = .168, t(2396) = 3.46, p = 5.49e-4, CI = [.073,.263]; CCW: slope = .29, t(2396) = 3.56, p = 3.81e-4, CI = [.131,.452]). We did not observe any interaction between the effect of the visual gain and the instruction.

Late muscular response

The second aspect studied with the EMG data was the late muscular response to the perturbations as a function of the visual perturbations for each instruction.
To do this, the late muscular activity was computed by averaging the muscle activity of the PD during trials against CW force field and of the PEC during trials against a CCW force field over a time window ranging from 300ms to 500ms after the movement onset. (See figure 4.1.6) Then the average baseline activity was subtracted and the mean across trials conditions was computed. The results are displayed in figure 4.1.8.

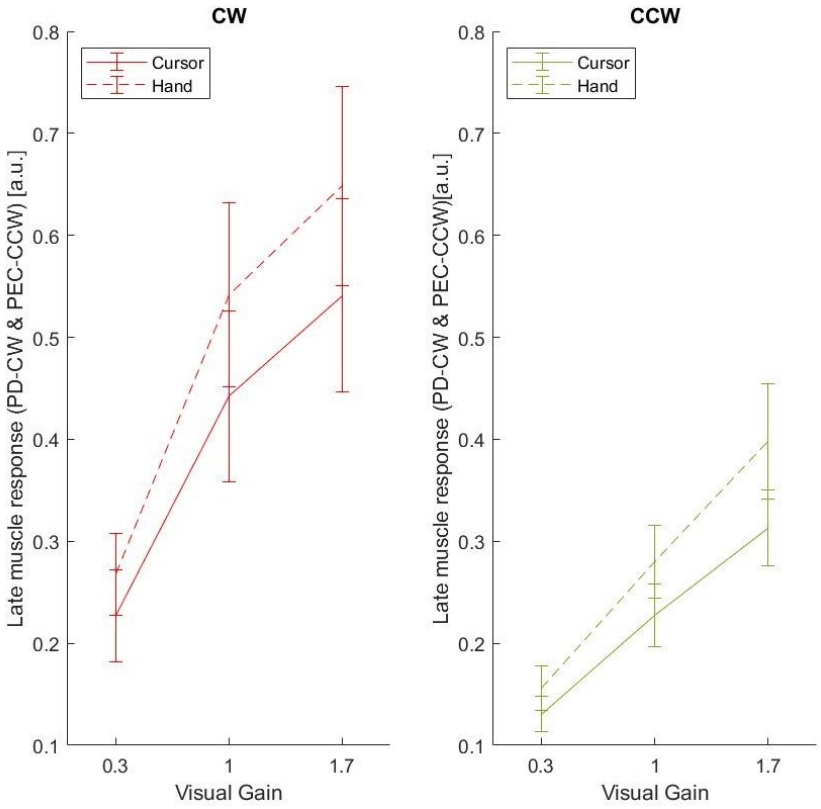

Figure 4.1.8 – Instruction comparison : Late muscular response across all participants. Average late EMG response for each force field direction as a function of visual gain. Each line indicates the across-participants average in each condition and the standard error of the means (SME) are shown with the vertical lines. Color-coding and linestyle follow the same convention as in figure 4.1.2.

We observed an increase of late muscle responses with the size of the visual gain for both force-field directions (CW: slope = .224, t(2396) = 5.52, p = 3.69e-8, CI = [.144,.303]; CCW: slope = .131, t(2396) = 5.98, p = 2.62e-9, CI = [.088,.175]). Further, muscle responses were significantly larger in the hand compared to the cursor instruction (CW: slope = .194, t(2396) = 2.94, p = 3.29e-3, CI = [.065,.324]; CCW: slope = .142, t(2396) = 3.96, p = 7.57e-5, CI = [.072,.212]). We did not observe any interaction between the effect of the visual gain and the instruction.

Baseline muscular activity

The last aspect studied from EMG data was the baseline activity for each muscle of interest during both instructions. The aim of this analysis is to see whether there was a baseline shift of the muscular activity between both instructions. To observe it, the across-participants average of muscular activity during baseline trials has been computed for the PEC and the PD muscles and plotted in the figure 4.1.9.

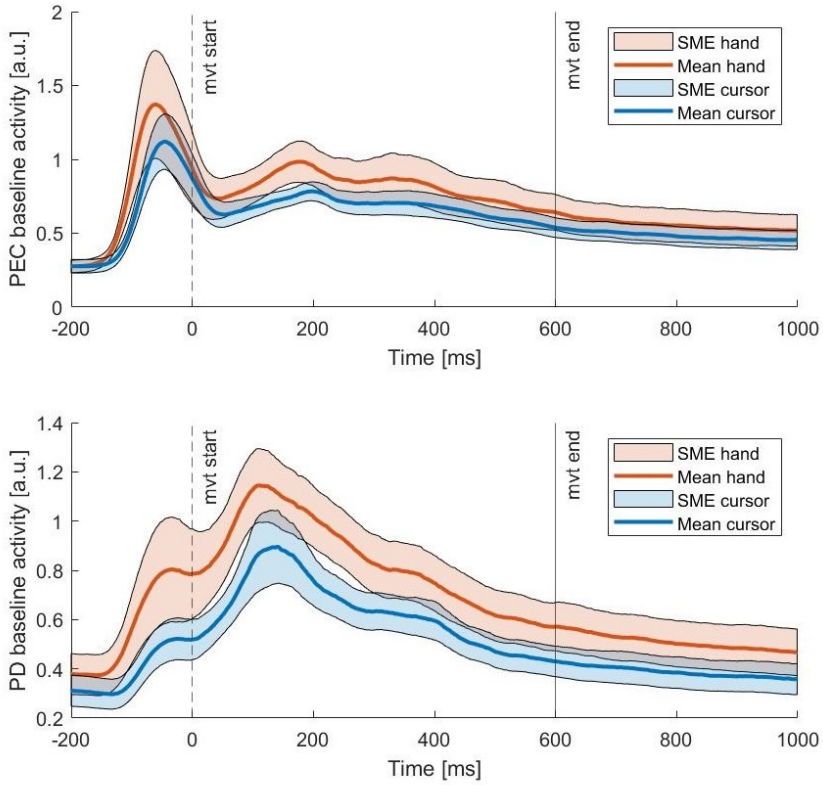

Figure 4.1.9 – Instruction comparison : Baseline EMG signals. The top panel represents the across-participants average muscular activity for the Pectoralis Major (PEC) during baseline trials. The orange curve represents the instruction in which participants were asked to control their hand. The blue one represents the instruction where they had to control the cursor. The shadowed areas are the standard errors for each curve. The bottom panel is the same as the top one but representing the activity of the Posterior Deltoid.

We observed no significant effect of the instruction on the mean PEC activity between movement start and movement hand during unperturbed trials ($p = .455$, $CI = [-.44,.2]$, $t(30) = -.76$, $SD = .44$) nor on the mean PD activity between movement start and movement hand ($p = .189$, $CI = [-.44,.091]$, $t(30) = -1.34$, $SD = .37$).

In view of these observations, it can be stated that the responses clearly scale with the size of the visual error and that they were larger when participants were instructed to control their hand instead of the cursor. Importantly, the instruction of whether to control hand or cursor did not impact the way participants considered the visual feedback.

4.2 Effect of the instruction order

As explained in section 3.2, half of the participants performed the cursor instruction block in the first position and the other half started with the hand instruction block. Given that the exposure to the first instruction might have influenced the behavior during the second instruction, it makes sense to also look at the participants' behavior separated by the order in which the instructions were performed.
In this section five variables will be analyzed : the endpoint error, the forward velocity, the early and late muscular responses and the task failure rate.

4.2.1 Kinematic data

Endpoint error

It has been shown in the previous section that we observed a significant decrease of the endpoint error when participants were asked to control their hand. The question is, was this outcome present regardless of the order in which the participants performed the two instructions? To answer that question the average endpoint error has been extracted for each group of participants having performed the instruction tasks in the same order and plotted in the figure 4.2.1.

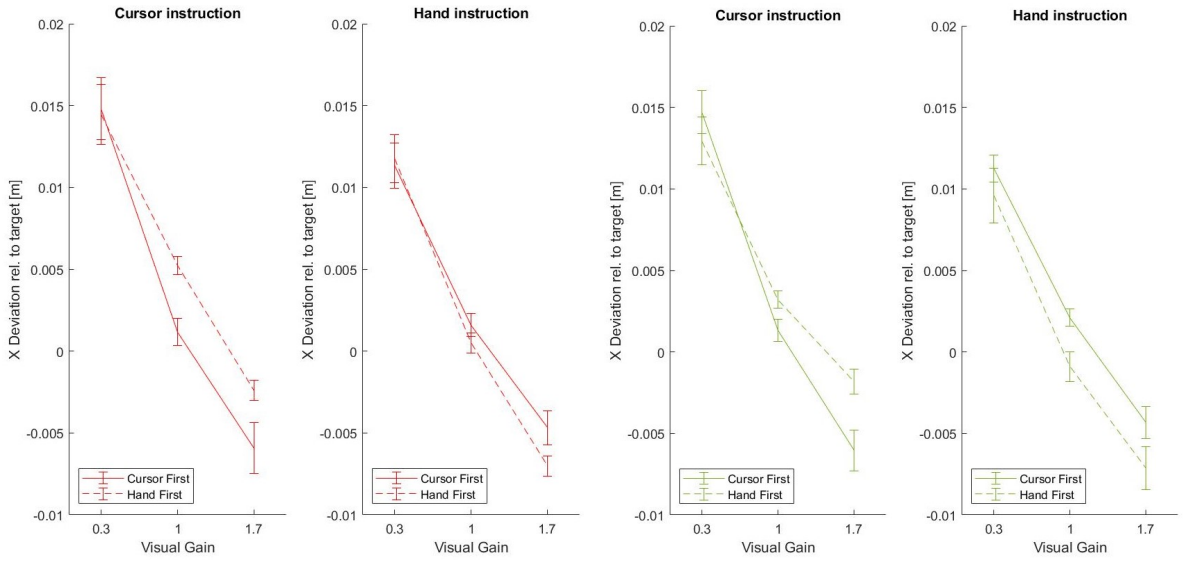

(a) Trials undergoing CW force-field

(b) Trials undergoing CCW force-field

Figure 4.2.1 – Instruction order comparison : Endpoint deviation relative to the target position Average endpoint deviation relative to the target position for each force field direction (CW:red , CCW:green) in each instruction as a function of visual gain. For this analysis, the sign of the lateral deviation for CCW trials has been changed such that for all trials, a positive deviation represents a greater deviation. Each line indicates the average across participants that have done the instruction blocks in the same order for each trial types and the standard error of the means (SME) are shown with the vertical lines. The endpoint deviation was computed the same way as for figure 4.1.3. In each subfigure, the left graph represents the endpoint error during the experiment where participants controlled the cursor and the right one where they controlled their hand. Dashed lines represent when participants had to control their hand during their first experiment while the thick ones represent the average across participants that began with the cursor controlling experiment.

There was no significant effect of the instruction order on the endpoint deviation for the hand instruction in both force field direction. However we observed a significant decrease of the endpoint error during the cursor instruction in CCW force field direction. (**CW :** *Cursor :* slope = -.0003, t(1196) = -.24, p = .8, CI = [-.003,.002] ; *Hand :* slope = -.0009, t(1196) = -.98, p = .32, CI = [-.002,.0009]. **CCW :** *Cursor :* slope = -.003, t(1196) = -2.3, p = .02, CI = [-.005,-.0004] ; slope = .002, t(1196) = 1.16, p = .25, CI = [-.001,.004]). We observed a significant interaction between the instruction order and the visual gain for cursor instruction in both force field directions but in only CW trials during hand instruction . (**CW :** *Cursor :* slope = .003, t(1196) = 3.18, p = .001, CI = [.001,.004] ; *Hand :* slope = .002, t(1196) = 2.29, p = .022, CI = [.0003,.004]. (**CCW :** *Cursor :* slope = .004, t(1196) = 6, p = 2.539e-9, CI = [.002,.006] ; *Hand :* slope = .0008, t(1196) = 1.23, p = .22, CI = [-.0005,.002].)

Maximum forward velocity

The second variable that has been analyzed in more details was the maximum forward velocity. In the previous section, it has been exposed that there was a significant increase

of the maximum forward velocity during CW trials when participants had to control their hand. The figure 4.2.2 displays the average maximum forward velocity across both participants' groups.

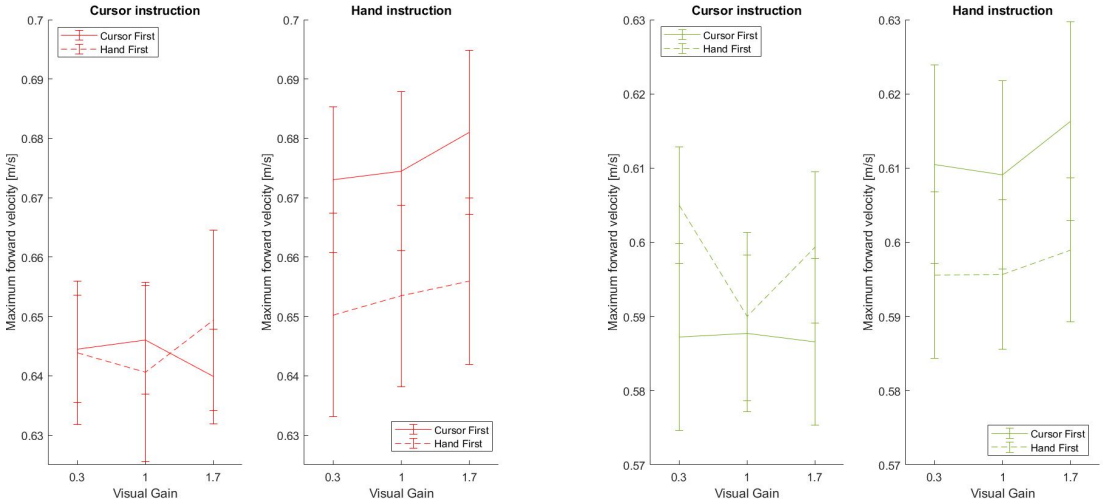

(a) Trials undergoing CW force-field

(b) Trials undergoing CCW force-field

Figure 4.2.2 – Instruction order comparison : Maximum forward velocity. Average peak of forward velocity for each force field direction in each instruction as a function of visual gain. Each line indicates the average across participants that have done the instruction blocks in the same order for each trial types and the standard error of the means (SME) are shown with the vertical lines. The endpoint deviation was computed the same way as for figure 4.1.4. In each subfigure, the left graph represents the maximum forward velocity during the experiment where participants controlled the cursor and the right one where they controlled their hand. Color-coding and linestyle follow the same convention as in figure 4.2.1.

There was no significant effect of the instruction order on the maximum forward velocity for both instructions and both force field directions (**CW :** *Cursor :* slope = -.0003, t(1196) = -.24, p = .8, CI = [-.003,.002] ; *Hand :* slope = -.0009, t(1196) = -.98, p = .32, CI = [-.002,.0009]. (**CCW :**) *Cursor :* slope = .014, t(1196) = .94, p = .34, CI = [-.016,.045] ; *Hand :* slope = .01, t(1196) = .77, p = .44, CI = [-.021,.048]).
Nor any interaction between the instruction order and the visual gain for both instructions and both force field directions (**CW :** *Cursor :* slope = .007, t(1196) = 1.06, p = .29, CI = [-.006,.021] ; *Hand :* slope = .002, t(1196) = .19, p = .84, CI = [-.014,.017]. (**CCW :** *Cursor :* slope = .-.004, t(1196) = -.54, p = .59, CI = [-.016,.009] ; *Hand :* slope = .002, t(1196) = .24, p = .81, CI = [-.012,.016]).

4.2.2 EMG data

Early muscular response

When comparing the average early muscular responses across all the participants, it has been observed that muscle responses were significantly larger in the hand compared to the

cursor instruction. The figure 4.2.3 shows the average early muscular response separated by instruction order.

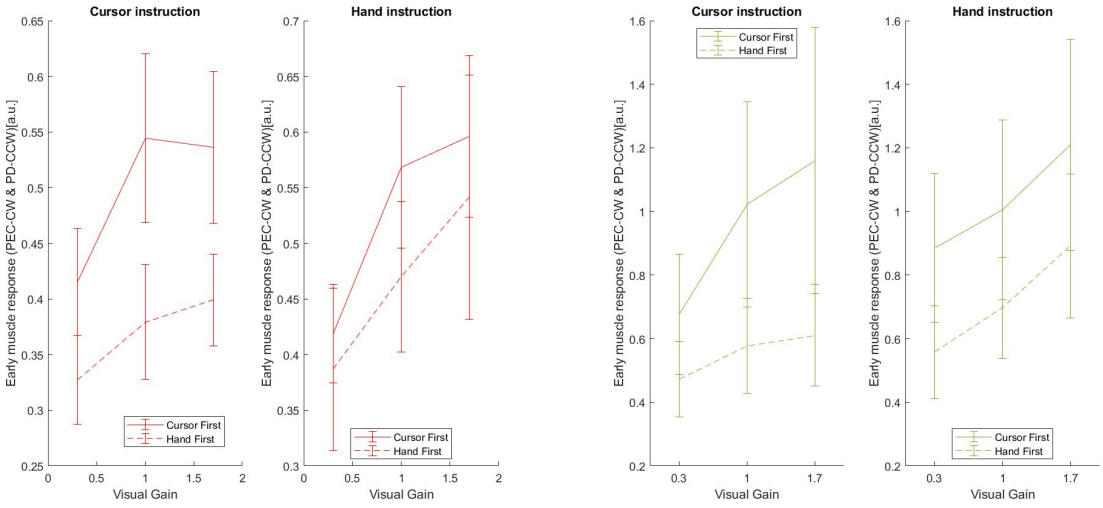

(a) Early CW

(b) Early CCW

Figure 4.2.3 – Instruction order comparison : Early muscular response. Average early muscular response for each force field direction in each instruction as a function of visual gain. Each line indicates the average across participants that have done the instruction blocks in the same order for each trial types and the standard error of the means (SME) are shown with the vertical lines. The early muscular response was computed the same way as for figure 4.1.7. In each subfigure, the left graph represents the maximum forward velocity during the experiment where participants controlled the cursor and the right one where they controlled their hand. Color-coding and linestyle follow the same convention as in figure 4.2.1.

There was no significant effect of the instruction order on the early muscular response for both instructions (**CW :** *Cursor :* slope = -.12, t(1196) = -.74, p = .46, CI = [-.42,.19]) ; *Hand :* slope = -.33, t(1196) = -.92, p = .35, CI = [-1.04,.37]. (**CCW :** *Cursor :* slope = -.35, t(1196) = -.85, p = .39, CI = [-1.15,.455]) ; *Hand :* slope = -.081, t(1196) = -.18, p = .86, CI = [-.974,.812]) .)
However, we observed a significant interaction between the instruction order and the visual gain during the cursor instruction in CCW force field direction (**CW :** *Cursor :* slope = -.02, t(1196) = .67, p = .50, CI = [-.07,.03]) ; *Hand :* slope = .02, t(1196) = .34, p = .73, CI = [-.11,.16]. (**CCW :** *Cursor :* slope = -.26, t(1196) = -4.05, p = 5.35e-5, CI = [-.389,-.135]); *Hand :* slope = -.055, t(1196) = -.54, p = .59, CI = [-.254,.144]).

Late muscular response

As for the early muscular response, late muscular responses to perturbations was higher when participants were asked to control their cursor. The figure 4.2.4 shows the average early muscular response separated by instruction order.

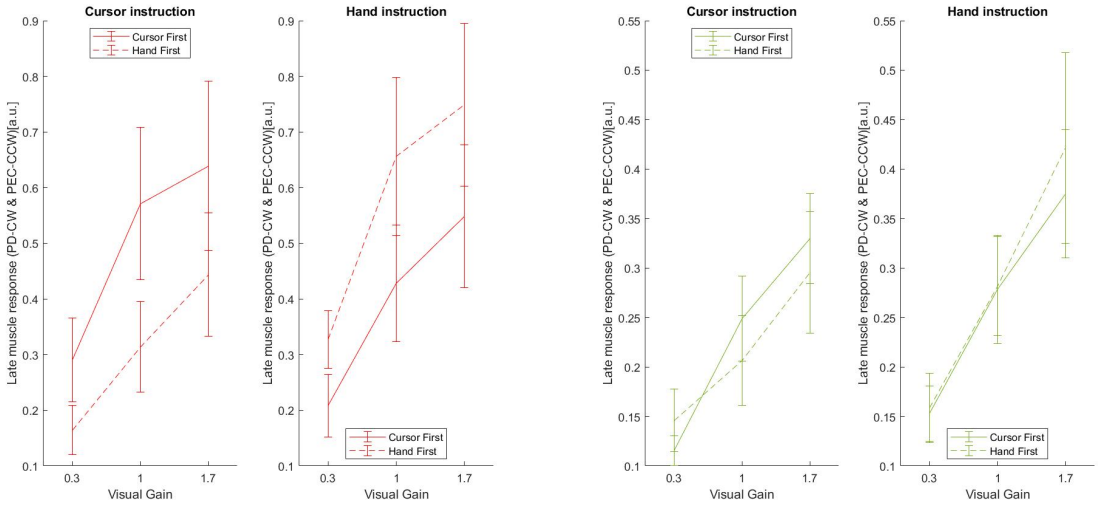

(a) Late CW

(b) Late CCW

Figure 4.2.4 – Instruction order comparison : Late muscular response. Average late muscular response for each force field direction in each instruction as a function of visual gain. Each line indicates the average across participants that have done the instruction blocks in the same order for each trial types and the standard error of the means (SME) are shown with the vertical lines. The late muscular response was computed the same way as for figure 4.1.8. In each subfigure, the left graph represents the maximum forward velocity during the experiment where participants controlled the cursor and the right one where they controlled their hand. Color-coding and linestyle follow the same convention as in figure 4.2.1.

There was no significant effect of the instruction order on the late muscular response for both instructions and both force field directions (**CW :** *Cursor :* slope = -.32, t(1196) = -1.26, p = .21, CI = [-.822,.179]) ; *Hand :* slope = -.46, t(1196) = -1.59, p = .11, CI = [-1.03,.11]) (**CCW :** *Cursor* :slope = -.004, t(1196) = -.02, p = .98, CI = [-.357,.349]) ; *Hand :* slope = -.24 , t(1196) = -.69, p = .49, CI = [-.919,.442]).
Nor any interaction between the instruction order and the visual gain for both instructions and both force field directions (**CW :** *Cursor :* slope = -.045, t(1196) = -.72, p = .47, CI = [-.167,.077]) ; *Hand :* slope = -.06, t(1196) = -.81, p = .416, CI = [-.209,.086]). (**CCW :** *Cursor :* slope = -.945, t(1196) = -1.79, p = .08, CI = [-.094,.004]) ; *Hand :* slope = -.029, t(1196) = -.635, p = .52, CI = [-.12,.061]).

4.2.3 Failure rate

The last aspect studied from the experimental data was the difficulty of each instruction for participants. For this purpose, the failure rate for each instruction has been calculated and averaged according to the order in which participants performed the instruction blocks. These values have been drawn as bar graphs on the figure 4.2.5.

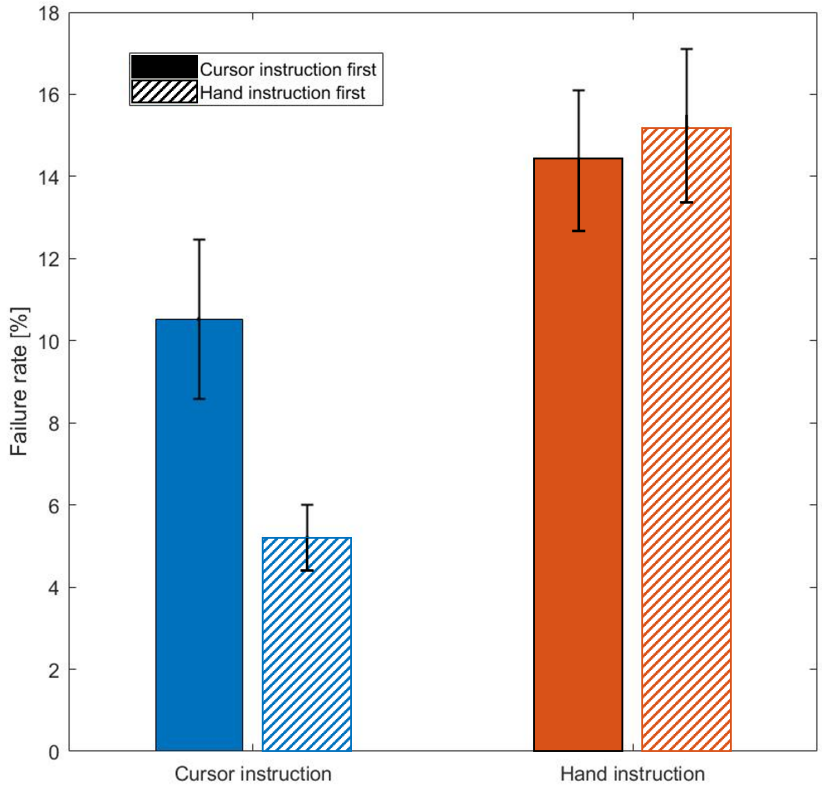

Figure 4.2.5 – Instruction order comparison : Failure rate. Average failure rate during both instructions. Each bar represents the average across participants that have done the instruction blocks in the same order. The first group represents the average across people who began with the cursor instruction and the second one represents the average across people who began with the hand instruction.

We observed a significant increase of failure rate when participants had to control the hidden hand instead of the visual cursor ($p = 2.45e\text{-}4$, $t(30) = -4.16$, $SD = 4.84$, $CI = [-10.62,-3.62]$). There was also a significant effect of the instruction order on the failure rate for the cursor instruction ($p = .0313$, $t(14) = 2.39$, $SD = 4.24$, $CI = [.525,9.626]$). However, the instruction order had no significant effect on the failure rate for the hand instruction ($p = .8813$, $t(14) = -.152$, $SD = 4.98$, $CI = [-5.72,4.96]$).

Given all these observations, it can be stated that the instruction order did not have a significant impact on the responses to perturbations. However, we observed a reduction in the failure rate when participants controlled the cursor after performing the hand instruction. Moreover, the instruction order implied a modification of the way visual gain was processed for the early muscular response and the endpoint error. Indeed, we observed that the corrective responses were smaller during the second task performed by the participants, independent of which one it was.

Chapter 5

Discussion

As explained in section 2.5, the aim of this thesis was to study whether the contribution of visual and proprioceptive feedback to movement control and adaptation is modulated by participants' awareness of whether or not the provided visual feedback can be deviated from their true hand location.
To this end, two experiments with the same protocol, but different instructions, were performed. Both experiments were subjected to mechanical perturbations and the lateral deviation of the cursor was multiplied by a gain to either increase or decrease the cursor deviation relative to the true deviation of the hand. In only one of these two experiments were participants aware of this visual gain.
Four main observations emerged from our analyses. First, regardless of the instruction given to participants, they integrated the visual feedback received, and their corrective responses increased with increasing visual error. Second, we observed larger responses when participants were instructed to control their hand. Also, the results showed that there was no significant change in adaptation between the two experiments. Finally, the study of failure rate showed that globally, the hand instruction task has been more difficult for participants.

Firstly, we observed a scaling of the responses with the visual gain for both instructions. Indeed, we found out that as visual gain increased, the lateral deviation relative to the target decreased and the muscle response increased.
This phenomenon illustrates that participants integrated the visual information in order to estimate the hand position as explained in section (2.4) even if the cursor deviated from the hidden hand location.
Moreover, this scaling observation was made in both experiments, meaning that even when the participants were told that it was possible for the cursor to be deviated, they continued to integrate the visual feedback to estimate their hand position.
As expressed in section 2.6, by asking participants to control their hand and informing them of a possible deviation of the cursor from the real hidden hand position, we expected

a dissociation of hand and visual cursor. Such dissociation would imply that the estimates of the cursor position and of the hand would also be updated separately, and that the estimation of the hand position would have been made only on the basis of proprioceptive feedback.
In our situation, it can accordingly be stated that participants were not able to ignore the visual feedback even if they were aware that it did not reliably represent their hand location.
This observation is consistent with the study made by Tsay & al. (2020) [34] in which they quantified participants' awareness of the motor adaptation occurring during sensorimotor adaptation. To do so, they conducted an experiment of reaching movements with "clamped" visual perturbations to a fixed angle different from zero. This kind of visual disturbance consists of a cursor that follows an invariant trajectory and is therefore unrelated to the participant's behavior. They observed that although participants were aware of the incongruency between their hand location and the visual feedback, an after effect occurred with them moving, in the opposite direction to the clamped visual feedback. Firstly, their results proved that participants were not aware of implicit sensorimotor adaptations, but they also showed that visual feedback had an impact on their subjective estimation of their own hand position. Another possible explanation for the participants' behavior would be the nature of the target used in our experiment. Indeed, some studies have shown that changing the modality of the target could influence the weighting of visual and proprioceptive information. For example, initially Sober & al (2005)[26] and later Cameron & al (2015) [35] studied reaching movements of participants under different target modalities (visual or proprioceptive). In both cases, their conclusion was that participants tended to have more confidence in sensory information being from the same modality as the target. This was in order to minimize the error induced by the frame change. Therefore, using a visual target as we did can justify the integration of the participants' visual signals despite the known deviation.

Secondly, we have seen that when participants were asked to control their hidden hand, the deviation relative to the targets' axis was smaller and their muscular responses were higher than when the instruction was to control the visual cursor. We also observed a greater forward velocity during the trials where participants controlled their hand. Moreover, we observed that this difference of behavior between instructions was present regardless of the order in which the participants performed it. However, we observed that participants integrated less the visual feedback for the motor correction during the second instruction performed.
A possible explanation for participants' behavior during the hand instruction task could be that they were not able to form an internal representation of the encountered perturbations (force and visual), and this might have led them to use a robust control strategy.

Similar to LQG control explained in section 2.1, robust control offers a mathematical description of a potential control strategy employed by the CNS. The important difference between these two models is that even if, as the LQG control, it relies on an internal model of the arm and the environment dynamics, the robust controller does not use an internal model of the perturbation. The aim of a robust control strategy is to be able to manage situations where disturbances in the environment are unpredictable and therefore cannot be learned by an internal model. Instead, the robust controller computes control commands assuming the worst-case perturbation. [36, 37]
Robust controller and LQG are solutions of the optimal feedback control problem. As explained in section 2.1, the motor command sent to the limb is computed based on a state estimation and feedback received from the system. When facing a perturbation, a corrective motor command will be applied. This corrective motor command is done at a factor called control gains. Changing the control gains modifies the sensitivity to the perturbations. In the robust control system, the perturbations faced are unpredictable, so the robustness of the controller has to be increased and this is made by increasing the control gains.
Crevecoeur & al (2019) [36] showed that this increase in control gains can be measured by a change in speed and sensitivity to external perturbations during trials. This has been shown respectively by an increase in forward velocity and muscular activity, as well as by a decrease of the after effects. They also observed smaller lateral deviations and velocities.
In our situation, a possible explanation of the participants' behavior is that they took the instruction to control their hand without being able to trust the visual cursor as a situation in which they could not model the disturbance. Thus, they may have applied a robust strategy to ensure that they could counteract these perturbations and perform the required movement correctly.
This theory could be supported by the results of the failure rate analysis as we found a clear difference between the two instructions. Indeed, the failure rate when participants had to control their hand was significantly higher than when they had to control the cursor. This could illustrate a higher difficulty that they translated into inability to model the environment. We also observed an increase in forward velocity and muscular activities that support this hypothesis. However, the after effects should have been smaller during hand training but this was not observed in our experiments.

Experiment limitations Some aspects of our experiments may have biased the observed results. First, the way in which the trials were randomized may have implied a bias in the way participants reacted to the disturbances. Indeed, as explained in section 3.2, each perturbed trial was followed by a baseline trial. This may have biased the adaptation analysis given that the participants were expecting a mechanical perturbation. Another

system of randomization could thus be considered.
Another limitation of our experiment was that the nuance created by the difference in instruction may have been too subtle for participants at times and they may not have grasped the difference between the two experiences at the outset. It might therefore be useful to think about an experiment involving more explicit proprioceptive control, such as changing the modality of the target, as done in the experiments of Sober & al [26] and Cameron & al [35].

Further perspectives As mentioned before, a question raised by our results is why participants integrated the visual feedback when they were aware of the cursor deviation from their hand position. To test the explanations proposed, some future experiments can be done. For example, we should replace the visual target by a proprioceptive one in order to see whether the modality of the target had an impact on the integration as suggested by Cameron & al (2015) [35] and Sober & al (2005) [26].
Although the hypothesis of a change of strategy between the two instructions holds true, this theory has to be tested with further experiments, and the question of the cause of this strategic change remains to be answered. For example, an adaptation that could be made to our current protocol would be to change the randomization system of the trials by making several baseline trials follow each other as in the experimental protocol used by Crevecoeur & al (2019) [36].

Chapter 6

Conclusion

The main goal of this master thesis was to analyze whether making explicit the non-alignment of the hand and the visual cursor would influence the way in which visual and proprioceptive feedback are integrated by the CNS during motor control and adaptation.

We had two initial hypotheses. Either the estimation of the hand position and the cursor position were combined, and thus the two sensory signals would be combined in a weighted way. Either the estimates of each would be updated separately, and thus the participants would be able to ignore the visual information and take into account only the proprioceptive signal.
Based on the theory of causal inference, we move towards the second hypothesis.

However, we have seen that participants were not able to ignore the visual feedback even if they were aware of its non-reliability and that they tended to have greater corrective responses when they had to control their hand rather than the visual cursor. Indeed, even when they were aware of the cursor deviation and were asked to control their hand, a reaction to the different visual gains was observed.

We hypothesized that when they were required to control their hand, participants were possibly not able to model the environment, leading them to change their motor control strategy to a robust control strategy.

Some future experiments, such as keeping the same trial protocol but changing the randomization system to make the system unpredictable or changing the target modality, can be conducted.

Bibliography

[1] Qinbiao Li, Jian Feng, Jia Guo, Zilin Wang, Puhong Li, Heshan Liu, and Zhijun Fan. Effects of the multisensory rehabilitation product for home-based hand training after stroke on cortical activation by using nirs methods. Neuroscience Letters, 717, 1 2020. ISSN 18727972. doi: 10.1016/j.neulet.2019.134682.

[2] Carlos Ramos, Paulo Novais, Céline Ehrwein, Nihan Juan, and M Corchado Rodríguez. Advances in intelligent systems and computing 291 ambient intelligence-software and applications. URL `http://www.springer.com/series/11156`.

[3] Stephen H. Scott. Optimal feedback control and the neural basis of volitional motor control, 2004. ISSN 1471003X.

[4] Donald E. Kirk. Optimal control theory : an introduction. 2004.

[5] Stephen H. Scott. A functional taxonomy of bottom-up sensory feedback processing for motor actions, 8 2016. ISSN 1878108X.

[6] Leonie Oostwoud Wijdenes and W. Pieter Medendorp. State estimation for early feedback responses in reaching: Intramodal or multimodal? Frontiers in Integrative Neuroscience, 11, 12 2017. ISSN 16625145. doi: 10.3389/fnint.2017.00038.

[7] Reza Shadmehr and Ferdinando A Mussa-Ivaldi. Adaptive representation of dynamics during learning of a motor task, 1994.

[8] Wolpert D. Kawato M. Internal models for motor control. Novartis Found Symp., 218:291–304, 1998. doi: 10.1002/9780470515563.ch16.

[9] Emanuel Todorov. Stochastic optimal control and estimation methods adapted to the noise characteristics of the sensorimotor system, 2005. URL `www.cogsci.ucsd.edu/`.

[10] Frédéric Crevecoeur. LGBIO2072 - mathematical models in neuroscience, 2021-2022.

[11] Frédéric Crevecoeur, Douglas P. Munoz, and Stephen H. Scott. Dynamic multisensory integration: Somatosensory speed trumps visual accuracy during feedback control. Journal of Neuroscience, 36:8598–8611, 8 2016. ISSN 15292401. doi: 10.1523/JNEUROSCI.0184-16.2016.

[12] Konrad P. Körding and Daniel M. Wolpert. Bayesian integration in sensorimotor learning. Nature, 427:244–247, 1 2004. ISSN 00280836. doi: 10.1038/nature02169.

[13] Marc O. Ernst and Martin S. Banks. Humans integrate visual and haptic information in a statistically optimal fashion. Nature, 415, 1 2002.

[14] Robert A. Scheidt, Michael A. Conditt, Emmanuele L. Secco, and Ferdinando A. Mussa-Ivaldi. Interaction of visual and proprioceptive feedback during adaptation of human reaching movements. J.Neurophysiol., 93:3200–3213, 1 2005. doi: 10.1152/jn.00947.2004.

[15] Robert A. Jacobs. What determines visual cue reliability? Trends in Cognitive Sciences, 6(8):345–350, 2002. ISSN 1364-6613. doi: https://doi.org/10.1016/S1364-6613(02)01948-4. URL https://www.sciencedirect.com/science/article/pii/S1364661302019484.

[16] Konrad P K and Joshua B Tenenbaum. Causal inference in sensorimotor integration.

[17] Konrad P. Körding, Ulrik Beierholm, Wei Ji Ma, Steven Quartz, Joshua B. Tenenbaum, and Ladan Shams. Causal inference in multisensory perception. PLoS ONE, 2, 9 2007. ISSN 19326203. doi: 10.1371/journal.pone.0000943.

[18] Reuben Rideaux, Katherine R Storrs, Guido Maiello, and Andrew E Welchman. How multisensory neurons solve causal inference. doi: 10.1073/pnas.2106235118/-/DCSupplemental. URL https://doi.org/10.1073/pnas.2106235118.

[19] Remi Gau and Uta Noppeney. How prior expectations shape multisensory perception. NeuroImage, 124:876–886, 1 2016. ISSN 10959572. doi: 10.1016/j.neuroimage.2015.09.045.

[20] Kunlin Wei and Konrad Körding. Relevance of error: What drives motor adaptation? Journal of Neurophysiology, 101:655–664, 2 2009. ISSN 00223077. doi: 10.1152/jn.90545.2008.

[21] Ladan Shams and Ulrik Beierholm. Bayesian causal inference: A unifying neuroscience theory. Neuroscience Biobehavioral Reviews, page 104619, 6 2022. ISSN 01497634. doi: 10.1016/j.neubiorev.2022.104619.

[22] Ladan Shams and Ulrik R. Beierholm. Causal inference in perception, 9 2010. ISSN 13646613.

[23] Tim Rohe and Uta Noppeney. Cortical hierarchies perform bayesian causal inference in multisensory perception. PLoS Biology, 13, 2015. ISSN 15457885. doi: 10.1371/journal.pbio.1002073.

[24] J.L. Taylor. Proprioception. In Larry R. Squire, editor, Encyclopedia of Neuroscience, pages 1143–1149. Academic Press, Oxford, 2009. ISBN 978-0-08-045046-9. doi: https://doi.org/10.1016/B978-008045046-9.01907-0. URL https://www.sciencedirect.com/science/article/pii/B9780080450469019070.

[25] Samuel J Sober and Philip N Sabes. Behavioral/systems/cognitive multisensory integration during motor planning. 2003.

[26] Samuel J. Sober and Philip N. Sabes. Flexible strategies for sensory integration during motor planning. Nature Neuroscience, 8:490–497, 4 2005. ISSN 10976256. doi: 10.1038/nn1427.

[27] Shoko Kasuga, Frédéric Crevecoeur, Kevin P. Cross, Parsa Balalaie, and Stephen H. Scott. Integration of proprioceptive and visual feedback during online control of reaching. Journal of Neurophysiology, 127:354–372, 2 2022. ISSN 15221598. doi: 10.1152/jn.00639.2020.

[28] Arman Sargolzaei, Mohamed Abdelghani, Kang K. Yen, and Saman Sargolzaei. Sensorimotor control: Computing the immediate future from the delayed present. BMC Bioinformatics, 17, 7 2016. ISSN 14712105. doi: 10.1186/s12859-016-1098-2.

[29] Jan Drugowitsch, Gregory C DeAngelis, Eliana M Klier, Dora E Angelaki, and Alexandre Pouget. Optimal multisensory decision-making in a reaction-time task. eLife, 3:e03005, jun 2014. ISSN 2050-084X. doi: 10.7554/eLife.03005. URL `https://doi.org/10.7554/eLife.03005`.

[30] Han Hou, Qihao Zheng, Yuchen Zhao, Alexandre Pouget, and Yong Gu. Neural correlates of optimal multisensory decision making under time-varying reliabilities with an invariant linear probabilistic population code. Neuron, 104:1010–1021.e10, 12 2019. ISSN 10974199. doi: 10.1016/j.neuron.2019.08.038.

[31] URL `https://brain.rehab.med.ubc.ca/kinarm/`.

[32] Zhaoxia Yu, Michele Guindani, Steven F. Grieco, Lujia Chen, Todd C. Holmes, and Xiangmin Xu. Beyond t test and anova: applications of mixed-effects models for more rigorous statistical analysis in neuroscience research, 1 2022. ISSN 10974199.

[33] R Shadmehr and FA Mussa-Ivaldi. Adaptive representation of dynamics during learning of a motor task. Journal of Neuroscience, 14(5):3208–3224, 1994. ISSN 0270-6474. doi: 10.1523/JNEUROSCI.14-05-03208.1994. URL `https://www.jneurosci.org/content/14/5/3208`.

[34] Jonathan S Tsay, Darius E Parvin, and Richard B Ivry. Continuous reports of sensed hand position during sensorimotor adaptation. J Neurophysiol, 124:1122–1130, 2020. doi: 10.1152/jn.00242.2020.-Sensorimotor. URL `www.jn.org`.

[35] Brendan D. Cameron and Joan López-Moliner. Target modality affects visually guided online control of reaching. Vision Research, 110:233–243, 5 2015. ISSN 18785646. doi: 10.1016/j.visres.2014.06.010.

[36] Frédéric Crevecoeur, Stephen H. Scott, and Tyler Cluff. Robust control in human reaching movements: A modelfree strategy to compensate for unpredictable disturbances. Journal of Neuroscience, 39:8135–8148, 10 2019. ISSN 15292401. doi: 10.1523/JNEUROSCI.0770-19.2019.

[37] Yuki Ueyama. Mini-max feedback control as a computational theory of sensorimotor control in the presence of structural uncertainty. Frontiers in computational neuroscience, 8:119, 09 2014. doi: 10.3389/fncom.2014.00119.

UNIVERSITÉ CATHOLIQUE DE LOUVAIN
École polytechnique de Louvain
Rue Archimède, 1 bte L6.11.01, 1348 Louvain-la-Neuve, Belgique | **www.uclouvain.be/epl**